Reply to the Editor's Decision for Manuscript hess-2018-83
"Geostatistical assessment of summertime rainfall observations in Korea based on composite precipitation and satellite water vapor data"

Editor Decision: *Publish subject to minor revisions (further review by editor)*

Comments to the Author: *This manuscript requires minor revisions as requested by three reviewers.*

$\Longrightarrow$ We have substantially revised the manuscript following the reviewers' comments. Please note that we have changed the title a little bit by modifying the expression "**summertime rainfall**" to "**warm-season precipitation**". Since we analyzed the data set in the period of April–October, we thought it was more appropriate to use "warm-season" rather than "summertime".

$\Longrightarrow$ The updated title in the revised manuscript is "**Geostatistical assessment of warm-season precipitation observations in Korea based on the composite precipitation and satellite water vapor data**".

Reply to the Comments by Referee #1 for Manuscript hess-2018-83 "Geostatistical assessment of summertime rainfall observations in Korea based on composite precipitation and satellite water vapor data"

General comments: *This manuscript assess the summertime rainfall characters in Korea via the geostatistical analyses on the composite precipitation and satellite water vapor data. Results show that the e-folding distance of precipitation ranges between 15 and 35 km while the e-folding time ranges between 1 and 2 h. The spatial autocorrelation has characteristic directionality. The results show that the current observational network with spation resolution of ∼13 km is difficult to capture the characteristic features of the localized heavy rainfall systems. It is also noted that the orographic effect is not assessed in this manuscript.*
The manuscript is well organized and I suggest accept with minor revision.

$\Longrightarrow$ We appreciate the positive comments by the referee. We have improved the manuscript by clearly describing some unclear sentences and figure captions. In the following, we made an item-by-item response to the specific comments by the referee.

Specific comments:

1) *Page 2, line 11-14, this sentence is too long.*

   $\Longrightarrow$ We have rewritten this part as:

   > Capturing the spatiotemporal features of precipitation systems from the observation networks is essential to runoff forecast, especially at the catchment scale and for the flooding cases (Volkmann et al., 2010).

2) *Page 12, line 9: "Korea" should not be subject.*

   $\Longrightarrow$ We have changed this part to:

   > Currently, the precipitation observation network in Korea has a spatial resolution of ∼13 km, distributing the analysis in an interval of 1 h.

3) *Page 27, in Figure 9 caption, a simple description of the case will be better, same for Fig 10–11.*

   $\Longrightarrow$ We have given a description of the case by including the precipitation type in each figure; however, we kept the information on time and date for each event because it is usually requested by the readers for the case studies. We have rewritten the figure's by reflecting other referee's comments as well. The modified captions, with new statements in bold, are as the followings:

   > Figure 9. **An LPMP case at 05 KST 25 August 2015:** (a) Precipitation distribution (source from https://afso.kma.go.kr/), (b) local $Z(G_i)$, (c) local Moran's I (I_i), and (d) Z-score of I_i. **The computational domain covers the area of** $34.34-38.97°$ **N and** $124.25-130.05°$ **E. Precipitation systems with maximum intensity and strong cluster characteristics** are marked by **the X symbols**, and the cold spots with dispersion pattern are denoted by

the arrow. **Non-precipitating areas have no color shading.**

Figure 10. Same as in Fig. 9 but **for an HPMP case at 17 KST 27 May 2013 and the computational domain of** 33.43 – 38.05°**N and** 124.25 – 130.04°**E**.

Figure 11. Same as in Fig. 9 but **for an HPFP case at 05 KST 24 October 2015 and the computational domain of** 37.14 – 39.06°**N and** 123.32 – 131.21°**E**.

Reply to the Comments by Referee #2 for Manuscript hess-2018-83
"Geostatistical assessment of summertime rainfall observations in Korea based on composite precipitation and satellite water vapor data"

Reviewer (Comments to Author):
This manuscript investigates the spatio-temporal characteristics of summer precipitation systems over the Korean peninsula through the geostatistical analysis using the combined datasets of ground observation and radar data. For the detailed analysis, they categorized the precipitation systems into four types based on the precipitation intensity (3mm/h) and ratio (20%) of precipitated stations. They found that the e-folding distance and time of precipitation systems are clearly dependent on the precipitation area, and directional pattern of precipitation systems. Also they found that the spatial distribution of water vapor has similar characteristics with precipitation but with strong spatial correlation over much longer distance (∼100 km), through the analysis of water vapor channel data of Himawari/Advanced Himawari Imager data. The results obtained in this study can be used for the detailed understanding of precipitation over South Korea. However, the manuscript should be improved in terms of additional analyses and scientific interpretation of results. Therefore, the manuscript needs to undergo a minor revision before being ready for publication in Hydrology and Earth System Sciences. Below I give some comments and suggestions that would help improving the manuscript.

$\Longrightarrow$ We appreciate the positive and valuable comments by the referee. We have substantially improved the manuscript by making some unclear statements clearer and by adding more discussions on detailed analyses and scientific interpretation, following the referee's comments. An item-by-item response to the referee's general and minor comments is provided below.

General comments:

1) *As we know that thresholds values are very important for the categorization (or clustering) precipitation systems. Please presents the background or ground of threshold values (3mm/h, 20%) used in this study.*

   $\Longrightarrow$ We agree with the referee that the threshold values are important for categorizing the precipitation systems. In order to determine the threshold values (i.e., 20 % and 3 mm h^{-1}), we have performed a preliminary statistical analysis of precipitation events (see Table R1 below). In classifying the precipitation types, we used two criteria — the portion of weather stations with precipitation (C1) and the station average precipitation rate (C2). We determined the threshold values when the cumulative percentage of each criterion reaches 80 % (see the red lines in Table R1). For example, in terms of C1, the cumulative percentage reaches 77.1 % with the portion of 10–20 % and 85.0 % with the portion of 20–30 %; thus selecting 20 % as the threshold value. In terms of C2, the cumulative percentage becomes 80.0 % with 2.0–2.9 mm h^{-1} and 93.3 % with 3.0–4.9 mm h^{-1}; thus choosing 3 mm h^{-1} as the threshold value. We have added the following statement at the early part of Sec. 2 in the revised manuscript, which also appears in the reply to item 2):

   > In order to determine the threshold values for classifying the precipitation types, we have conducted a preliminary statistical analysis on precipitation

events in the period of 2011–2015 (not shown). As the precipitation events occur in a given time period and/or space interval, our precipitation data are assumed to follow the Poisson distribution, which represents a probability situation of a large number of observation with a small probability of occurrence. Many studies developed the Poisson distribution models to estimate rainfall and cluster the rainfall systems (e.g., Rodriguez-Iturbe et al., 1987; Lee et al., 2014; Barton et al., 2016; Ritschel et al., 2017). We have chosen the threshold values when the cumulative percentage of precipitation events for each criterion (i.e., C1 and C2) reached approximately 80 %; thus obtaining the threshold values of 20 % for C1 and 3 mm h^{-1} for C2, respectively.

2) *The domain of data mentioned in the 2 Data description is not well matched with the analysis results (e.g., Figure 1)*

$\Longrightarrow$ We appreciate the referee for pointing this out, and we admit that our data description and Fig. 1 might have caused confusion. We have used the station data, as shown in Fig. 1, to classify the precipitation types (see Table R1 below); we have utilized the 1 km composite precipitation data for the precipitation analyses, including spatial correlations. We actually noticed that Fig. 1 should be updated because the station precipitation data were obtained from three observation networks with a total of 688 stations — the Automated Synoptic Observing Systems (ASOS), the Automatic Weather Stations (AWS), and Automated Agriculture Observing System (AAOS). We also noticed that the information on the radar locations and coverages would be essential because both the station and radar data were used to produce the 1 km composite precipitation data. In the revised manuscript, we modified Fig. 1 by updating the weather station locations and by including the radar locations and coverages (see Fig. R1 below). We have rewritten the text by clearly describing the data used in this study. We first modified the beginning sentences in the second paragraph of Sec. 1, with new statements in bold, as:

> "The ground-based rainfall observation data, in Korea, are collected from the Automated Synoptic Observing Systems (ASOS), the Automatic Weather Stations (AWS), **and the Automated Agriculture Observing System (AAOS)**. The observation density is about 67 km for ASOS and approximately 13 km by including AWS. **The agrometeorological observation network consists of 11 AAOS stations (Choi et al., 2015).** ···"

$\Longrightarrow$ We have also modified and reorganized the early part of Sec. 2, by including the step-by-step description of the method to produce the composite precipitation data, as (new sentences in bold):

> **We use the precipitation data from weather stations (see Fig. 1) to categorize the precipitation systems.** We classify four different precipitation types statistically, based on two criteria: the portion of weather stations with precipitation (C1), and the station average precipitation rate (C2). **In order to determine the threshold values for classifying the precipitation types, we have conducted a preliminary statistical analysis on precipitation events in the period of 2011–2015 (not shown). As the precipitation events occur in a given time period and space interval, our precipitation data are assumed to follow the Poisson distribution,**

which represents a probability situation of a large number of observation with a small probability of occurrence. Many studies developed the Poisson distribution models to estimate rainfall and to cluster the rainfall systems (e.g., Rodriguez-Iturbe et al., 1987; Lee et al., 2014; Barton et al., 2016; Ritschel et al., 2017). We have chosen the threshold values when the cumulative percentage of precipitation events for each criterion (i.e., C1 and C2) reached approximately 80 %; thus obtaining the threshold values of 20 % for C1 and 3 mm h^{-1} for C2, respectively. Our preliminary statistical analysis showed that, in general, most precipitation events occur over small areas and precipitation events with high intensity rarely occur over large areas. The locality of precipitation appeared higher as the precipitation intensity were higher, in accordance with Nam et al. (2014). In particular, precipitation systems with the highest intensity ($\geq$ 10 mm h^{-1}) were mostly confined to a small area with the number of stations less than 10 % of total weather stations. This implies that the locality feature of precipitation systems may depend on the threshold value in precipitation intensity.

Based on these criteria, we define four different precipitation types, as shown in Table 1: 1) Low Precipitation at a Few Points (LPFP) for C1 $<$ 20 % and C2 $<$ 3 mm h^{-1}; 2) Low Precipitation at Many Points (LPMP) for C1 $\geq$ 20 % and C2 $<$ 3 mm h^{-1}; 3) High Precipitation at a Few Points (HPFP) for C1 $<$ 20 % and C2 $\geq$ 3 mm h^{-1}; and 4) High Precipitation at Many Points (HPMP) for C1 $\geq$ 20 % and C2 $\geq$ 3 mm h^{-1}. We practically exclude the LPFP type in our analyses, i.e., the case with C1 $<$ 20 % and C2 $<$ 3 mm h^{-1}, because it may be less effective.

The Korea Meteorological Administration (KMA) has produced the composite precipitation data over Korea **using the data from radars, weather stations and satellites, through the following steps (see Hwang et al., 2015): 1) remove non-precipitation echoes from the radar data using the satellite cloud type data; 2) calculate the difference between the station precipitation and the radar estimated precipitation; 3) perform the objective analysis on the precipitation difference field and on the station precipitation data; 4) correct the bias using the objectively-analyzed difference field; and 5) combine the corrected radar-estimated precipitation data and the objectively-analyzed station precipitation data to produce the composite precipitation data (in mm h^{-1}). In order to analyze the precipitation systems with the evenly distributed high-resolution data, we used these composite precipitation data, which cover** 1153 km $\times$ 1441 km over the Korean Peninsula, with a grid size of 1 km and a time resolution of 1 h. Geostatistical analyses are conducted using the composite precipitation data sets from April to October in a period of 2013–2015 to investigate the spatial and temporal characteristics of summer rainfall.

3) *The author should mention about the sensitivity of analysis results to the threshold values for the categorization of precipitation systems.*

$\Longrightarrow$ As shown in Table R1, heavy precipitation systems have high locality; especially, precipitation with the highest intensity (≥ 10 mm h^{-1}) mostly occurs in a small area with the number of stations less than 10 % of total weather stations. This is consistent with the findings of Nam et al. (2014), and implies that the precipitation analysis results may depend on (be sensitive to) the threshold values. We have added the following sentence to next to the newly-added paragraph in item 1) above (see also the reply to item 2):

> Our preliminary statistical analysis showed that, in general, most precipitation events occur over small areas and precipitation events with high intensity rarely occur over large areas. The locality of precipitation appeared higher as the precipitation intensity were higher, in accordance with Nam et al. (2014). In particular, precipitation systems with the highest intensity (≥ 10 mm h^{-1}) were mostly confined to a small area with the number of stations less than 10 % of total weather stations. This implies that the locality feature of precipitation systems may depend on the threshold value in precipitation intensity.

4) *It will be helpful for the understanding of the single cell storms marked by X in Figures 9 and 10 if the authors presents the background for the marking.*

$\Longrightarrow$ We appreciate the referee for pointing this out. We think the expression "single cell storms" is not appropriate here. We originally intended to put the "X" marks on the locations of precipitation systems with maximum intensity (precipitation rate) and strong cluster characteristics. To avoid any confusion, we have modified the captions of Figs. 9 and 10 accordingly. By reflecting the referee's suggestion in Minor comments (items 3 and 4) and other referee's comments as well, the captions are rewritten as:

> Figure 9. **An LPMP case at 05 KST 25 August 2015:** (a) Precipitation distribution (source from https://afso.kma.go.kr/), (b) local $Z(G_i)$, (c) local Moran's I (I_i), and (d) Z-score of I_i. **The computational domain covers the area of** $34.34-38.97°$ **N and** $124.25-130.05°$ **E. Precipitation systems with maximum intensity and strong cluster characteristics** are marked by **the X symbols**, and the cold spots with dispersion pattern are denoted by the arrow. **Non-precipitating areas have no color shading.**
>
> Figure 10. Same as in Fig. 9 but **for an HPMP case at 17 KST 27 May 2013 and the computational domain of** $33.43-38.05°$**N and** $124.25-130.04°$**E.**

$\Longrightarrow$ We have also rewritten the statement in page 10, line 11 as:

> Figure 9c depicts **several precipitation systems with maximum intensity (i.e., precipitation rate; see Fig. 9a)** in the cluster area (marked by **the X symbols**). **These systems show the highest local Moran's I with the spatial scale of less than 30 km.** The cluster patterns were statistically significant at a significance level of 0.01 (Fig. 9d). $\cdots\cdots$ The map of local Moran's I shows that **a precipitation system with a strong cluster feature has developed**, over the southwestern sea of the Korean Peninsula, along with the successive cluster patterns **in a line type** (Fig. 10c), with a significance level of 0.01 (Fig. 10d).

Minor comments:

1) *The location of AWS is not correct in Figure 1.*

$\Longrightarrow$ We have redrawn Fig. 1 in the revised manuscript (see Fig. R1 below).

2) *I think that the number of y axis in Figures 5 and 8 is km. So, give the unit in Figures 5 and 8.*

$\Longrightarrow$ We appreciate the referee for pointing this out. We now have explicitly given the unit (km) in the captions of Figs. 5 and 8. We also changed the name of diagram to "radar chart" from "radar diagram" to avoid any confusion. The captions of Figs. 5 and 8 are rewritten, and the cation of Fig. 8 also reflects the referee's suggestion in items 3) and 4):

> Figure 5. A radar **chart** representing the directional e-folding distance **(in km) for each precipitation type** at the mode in **the directional histogram (not shown) depicting the number of cases according to the e-folding distance in different directions**.

> Figure 8. A radar **chart** representing the directional e-folding distance **(in km)** of brightness temperature of **the Himawari/AHI** water vapor band **8, 9 and 10** at the mode in the histogram of case numbers for **LPMP (solid), HPMP (dashed), and HPFP (dotted). The colors indicate autocorrelation coefficients of 0.7 (blue), 0.8 (black), and 0.9 (grey), respectively**.

3) *Figure 6. The averaged spatial autocorrelation of brightness temperature of water vapor band (a) 8, (b) 9, and (c) 10 for each precipitation ⇒ The averaged spatial autocorrelation of brightness temperature of water vapor band (a) 8, (b) 9, and (c) 10 Himawari/AHI for each precipitation*

$\Longrightarrow$ The caption of Fig. 6 is now modified following the referee's suggestion as:

> Figure 6. The averaged spatial autocorrelation of brightness temperature of **the Himawari/AHI** water vapor band (a) 8, (b) 9, and (c) 10 for each precipitation type.

4) *Some index of figures are not clear (e.g., Figures 7, 8, 9, 10, and 11).*

$\Longrightarrow$ We have rewritten the captions, by reflecting suggestions by other referees as well. The revised captions appear as the followings:

> Figure 7. The average directional spatial autocorrelation of the brightness temperature of **the Himawari/AHI** water vapor band **8, 9 and 10** by each precipitation type **(i.e., HPFP, HPMP, and LPMP) for directions of** 0° **(black),** 45° **(blue),** 90° **(red), and** 135° **(green). The direction (angle) is measured counterclockwise from the origin-east axis (i.e.,** 0°).

> Figure 8. A radar **chart** representing the directional e-folding distance **(in km)** of brightness temperature of **the Himawari/AHI** water vapor band **8, 9 and 10** at the mode in the histogram of case numbers for **LPMP (solid), HPMP (dashed), and HPFP (dotted). The colors indicate autocorrelation coefficients of 0.7 (blue), 0.8 (black), and 0.9 (grey), respectively**.

Figure 9. **An LPMP case at 05 KST 25 August 2015:** (a) Precipitation distribution (source from https://afso.kma.go.kr/), (b) local $Z(G_i)$, (c) local Moran's I (I_i), and (d) Z-score of I_i. **The computational domain covers the area of** $34.34-38.97°$ **N and** $124.25-130.05°$ **E. Precipitation systems with maximum intensity and strong cluster characteristics** are marked by **the X symbols**, and the cold spots with dispersion pattern are denoted by the arrow. **Non-precipitating areas have no color shading.**

Figure 10. Same as in Fig. 9 but **for an HPMP case at 17 KST 27 May 2013 and the computational domain of** $33.43 - 38.05°$**N and** $124.25 - 130.04°$**E**.

Figure 11. Same as in Fig. 9 but **for an HPFP case at 05 KST 24 October 2015 and the computational domain of** $37.14 - 39.06°$**N and** $123.32 - 131.21°$**E**.

5) *Check the order of references (e.g., Cassardo, ..., Carruthers, ...; Smith, ..., Skojen, ...).*

$\Longrightarrow$ We have corrected the order of references in the revised manuscript.

Table R1. Preliminary statistical analysis of precipitation events during 2011–2015 by two criteria – the portion of weather stations with precipitation and the station average precipitation rate. The red lines indicate the boundaries when the cumulative percentage of precipitation events is approximately 80 %.

		The portion of weather stations with precipitation (%)												
		0-10	10-20	20-30	30-40	40-50	50-60	60-70	70-80	80-90	90-	Sum	Percentage (%)	Cumulative percentage (%)
The station average precipitation rate (mm/h)	0.1-0.9	5241	399	156	60	29	5	2	1	0	0	5893	40.0	40.0
	1.0-1.9	2238	665	383	235	148	99	57	33	18	6	3882	26.3	66.3
	2.0-2.9	891	352	262	196	109	89	48	35	29	12	2023	13.7	80.0
	3.0-4.9	765	322	224	212	159	85	77	43	49	35	1971	13.4	93.3
	5.0-9.9	317	118	116	115	76	47	35	19	18	8	869	5.9	99.2
	10.0-	61	6	19	11	14	1	0	0	0	0	112	0.8	100.0
	Sum	9513	1862	1160	829	535	326	219	131	114	61	14750		
	Percentage (%)	64.5	12.6	7.9	5.6	3.6	2.2	1.5	0.9	0.8	0.4			
	Cumulative percentage (%)	64.5	77.1	85.0	90.6	94.2	96.4	97.9	98.8	99.6	100.0			

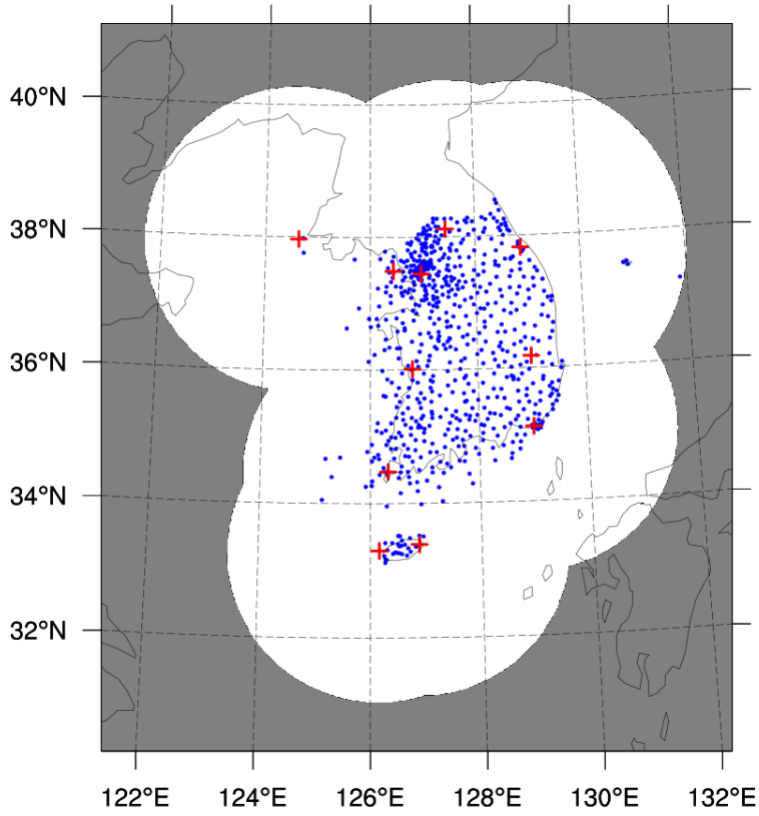

Figure R1. The weather station locations (blue dots) and radar locations (red "+" symbols) and coverages (white area) in Korea.

References

Barton, Y., Giannakaki, P., Von Waldow, H., Chevalier, C., Pfahl, S., and Martius, O.: Clustering of regional-scale extreme precipitation events in Southern Switzerland, Mon. Wea. Rev., 144, 347–369, 2016.

Choi, S.-W., Lee, S.-J., Kim, J. Lee, B.-L., Kim, K.-R., and Choi, B.-C.: Agrometeorological observation environment and periodic report of Korea Meteorological Administration: Current status and suggestions, Korean J. Agric. For. Meteorol., 17, 144–155, doi:10.5532/KJAFM.2015.17.2.144, 2015 (in Korean with English abstract).

Lee, J., Yoon, J., and Jun, H. D.: Evaluation for the correction of radar rainfall due to the spatial distribution of raingauge network, J. Korea Soc. Hazard Mitig., 14, 337–345, http://dx.doi.org/10.9798/KOSHAM.2014.14.6.337, 2014 (in Korean with English abstract).

Nam, J.-E., Lee, Y. H., Ha, J.-C., and Cho, C.-H.: A study on the e-folding distance of summer precipitation using precipitation reanalysis data, in: Proc. the Autumn Meeting of Korean Meteorological Society, 2014, Korean Meteorol. Soc., Jeju, Korea, 13–15 October 2014, 657–658, 2014.

Ritschel, C., Ulbrich, U., Névir, P., and Rust, H. W.: Precipitation extremes on multiple timescales — Bartlett-Lewis rectangular pulse model and intensity-duration-frequency curves, Hydrol. Earth Syst. Sci., 21, 6501–6517, https://doi.org/10.5194/hess-21-6501-2017, 2017.

Rodriguez-Iturbe, I., Cox, D. R., and Isham, V.: Some models for rainfall based on stochastic point processes, Proc. R. Soc. London, Ser. A, 410, 269–288, 1987.

Reply to the Comments by Referee #3 for Manuscript hess-2018-83
"Geostatistical assessment of summertime rainfall observations in Korea based on composite precipitation and satellite water vapor data"

This study classifies rainfall systems in Korea on the basis of their spatiotemporal structures by analyzing the observed precipitation, water vapor and cloud data. The subject is of an interest to not only to meteorologists but also to hydrologists. The paper is well organized but needs improvements before it can be accepted for publication. It also needs substantial improvements in writing.

$\Longrightarrow$ We appreciate the positive and valuable comments by the referee, which helped us improve the quality of the manuscript. We have faithfully revised the manuscript following the referee's specific comments, including some corrections and suggestions. We have also rewritten many parts of the manuscript, trying to avoid any confusion, especially in description of data and interpretation of results. In the following, we made an item-by-item response to the specific comments by the referee.

Below are my specific comments:

(1) *It looks that the rainfall analysis utilizes only the 1-km KMA analysis data. If so, Fig. 1 may not be needed - it can confuse some readers. Please see the comment (2) below for related concerns.*

$\Longrightarrow$ As the referee pointed out, for our rainfall analyses, we have utilized the 1 km composite precipitation data, which were based on both the station and radar data. However, in classifying the precipitation types (see Table R1 below), we have used the station data only, and included Fig. 1. We actually noticed that Fig. 1 should be updated because the station precipitation data included the data from three observation networks with a total of 688 stations — the Automated Synoptic Observing Systems (ASOS), the Automatic Weather Stations (AWS), and Automated Agriculture Observing System (AAOS). We also noticed that the information on the radar locations and coverages would be essential because both the station and radar data were used to produce the 1 km composite precipitation data. In the revised manuscript, we modified Fig. 1 by updating the weather station locations and by including the radar locations and coverages (see Fig. R1 below). We have rewritten the text by clearly describing the data used in this study. We have modified the beginning sentences in the second paragraph of Sec. 1, with new statements in bold, as:

> "The ground-based rainfall observation data, in Korea, are collected from the Automated Synoptic Observing Systems (ASOS), the Automatic Weather Stations (AWS), **and the Automated Agriculture Observing System (AAOS)**. The observation density is about 67 km for ASOS and approximately 13 km by including AWS. **The agrometeorological observation network consists of 11 AAOS stations (Choi et al., 2015).** ..."

See also the early part of Sec. 2, and the authors' reply to the referee's comments (2) below.

(2) *Page 20, line 24: "the portion of weather stations" → not clear what "weather stations" imply here. If this implies the 600 real stations in Fig. 1, the authors have to provide how they*

applied their analysis tools to the irregularly distributed stations. If it implies each grid points of the KMA analysis, this must be indicated ("grid points" instead of "weather stations") and delete Fig. 1.

$\Longrightarrow$ We assume that the referee meant for "Page 3, line 24". Here, the "weather stations" imply the real weather stations (i.e., ASOS + AWS + AAOS; see Fig. R1). As mentioned in (1), we used the weather station data to classify the precipitaion types. The base data for classification is shown in Table R1 below (not included in the revised manuscript). The 1 km composite data are produced using the radar, station and satellite data, through the method described in Hwang et al. (2015) — see also the step-by-step description below. We have rewritten the first and second paragraphs in Sec. 2, with new statements in bold, and reorganized it as:

> **We use the precipitation data from weather stations (see Fig. 1) to categorize the precipitation systems.** We classify four different precipitation types statistically, based on two criteria: the portion of weather stations with precipitation (C1), and the station average precipitation rate (C2). **In order to determine the threshold values for classifying the precipitation types, we have conducted a preliminary statistical analysis on precipitation events in the period of 2011–2015 (not shown). As the precipitation events occur in a given time period and space interval, our precipitation data are assumed to follow the Poisson distribution, which represents a probability situation of a large number of observation with a small probability of occurrence. Many studies developed the Poisson distribution models to estimate rainfall and to cluster the rainfall systems (e.g., Rodriguez-Iturbe et al., 1987; Lee et al., 2014; Barton et al., 2016; Ritschel et al., 2017). We have chosen the threshold values when the cumulative percentage of precipitation events for each criterion (i.e., C1 and C2) reached approximately 80 %; thus obtaining the threshold values of 20 % for C1 and 3 mm h^{-1} for C2, respectively. Our preliminary statistical analysis showed that, in general, most precipitation events occur over small areas and precipitation events with high intensity rarely occur over large areas. The locality of precipitation appeared higher as the precipitation intensity were higher, in accordance with Nam et al. (2014). In particular, precipitation systems with the highest intensity ($\geq$ 10 mm h^{-1}) were mostly confined to a small area with the number of stations less than 10 % of total weather stations. This implies that the locality feature of precipitation systems may depend on the threshold value in precipitation intensity.**
>
> Based on these criteria, we define four different precipitation types, as shown in Table 1: 1) Low Precipitation at a Few Points (LPFP) for C1 $<$ 20 % and C2 $<$ 3 mm h^{-1}; 2) Low Precipitation at Many Points (LPMP) for C1 $\geq$ 20 % and C2 $<$ 3 mm h^{-1}; 3) High Precipitation at a Few Points (HPFP) for C1 $<$ 20 % and C2 $\geq$ 3 mm h^{-1}; and 4) High Precipitation at Many Points (HPMP) for C1 $\geq$ 20 % and C2 $\geq$ 3 mm h^{-1}. We practically exclude the LPFP type in our analyses, i.e., the case with C1 $<$ 20 % and C2 $<$ 3 mm h^{-1}, because it may be less effective.
>
> The Korea Meteorological Administration (KMA) has produced the com-

posite precipitation data over Korea **using the data from radars, weather stations and satellites, through the following steps (see Hwang et al., 2015): 1) remove non-precipitation echoes from the radar data using the satellite cloud type data; 2) calculate the difference between the station precipitation and the radar estimated precipitation; 3) perform the objective analysis on the precipitation difference field and on the station precipitation data; 4) correct the bias using the objectively-analyzed difference field; and 5) combine the corrected radar-estimated precipitation data and the objectively-analyzed station precipitation data to produce the composite precipitation data (in mm h^{-1}). In order to analyze the precipitation systems with the evenly distributed high-resolution data, we used these composite precipitation data, which cover** 1153 km × 1441 km over the Korean Peninsula, with a grid size of 1 km and a time resolution of 1 h. Geostatistical analyses are conducted using the composite precipitation data sets from April to October in a period of 2013–2015 to investigate the spatial and temporal characteristics of summer rainfall.

(3) *Provide the formulation of the weighting function $w_{ij}(d)$ in Eq. (7) and explain why the specific form is selected to represent the spatial variations.*

$\Longrightarrow$ We used an inverse distance weighting (IDW) function, i.e., $w_{ij}(d) = 1/d_{ij}$ where d_{ij} is the distance between grids i and j. In fact, this is the same as the one used in calculating Moran's I (see Eqs. (4) and (5)). The IDW is a widely-used one among the spatial weighting functions. We have modified the sentence that defines w_{ij} (page 5, line 20, below Eq. (4), in the original manuscript) as (the modified parts in bold):

> "$\cdots$ Here, w_{ij} is the spatial weight of the link between i and j, which is defined by the inverse distance weight**, i.e., $w_{ij} = 1/d_{ij}$ with d_{ij} representing the distance between grids i and j.** $\cdots$"

We have also modified the expression right below Eq. (7) as (the modified parts in bold):

> "where d is the distance between the target feature and the neighboring feature**, and w_{ij} is the same spatial weight (i.e., the inverse distance weight) used for calculating Moran's I as in Eqs. (4) and (5)**. $\cdots$"

(4) *Page 7, line 20: This result is trivial consequence of classifying the precipitation system in terms of a number of data points; if rainfall occurs only over a small number of points, its spatial scale is limited by design. Their selection of 3 mm/h as the threshold value between heavy and light precipitation may cause the lack of relationship between precipitation intensity and spatial scales. Nam et al. may be a good reference for this. In fact, this result can depend on the selection of the threshold value. The authors need to explain the choice of 3 mm/h as the threshold.*

$\Longrightarrow$ The threshold values (i.e., 20 % and 3 mm h^{-1}) were taken based on a preliminary statistical analysis of precipitation events, as shown in Table R1. Since we are dealing with precipitation occurrences for a given time period and/or space interval, our data mostly follow the Poisson distribution. In classifying the precipitation types, we used two criteria — the portion of weather stations with precipitation and the station average precipitation rate — and determined the threshold values when the cumulative

percentage of each criterion reaches 80 % (see the red lines in Table R1). In terms of the portion of weather stations with precipitation, the cumulative percentage reaches 77.1 % with the portion of 10–20 % and 85.0 % with the portion of 20–30 %; thus selecting 20 % as the threshold value. In terms of the station average precipitation rate, the cumulative percentage becomes 80.0 % with 2.0–2.9 mm h^{-1} and 93.3 % with 3.0–4.9 mm h^{-1}; thus choosing 3 mm h^{-1} as the threshold value. As we have selected 3 mm h^{-1} as the threshold value based on this statistical analysis, this selection may not cause a lack of relationship between precipitation intensity and spatial scales. Actually Table R1 shows that heavy precipitation systems have high locality, which is consistent with the findings of Nam et al. (2014). Especially precipitation with the highest intensity ($\geq$ 10 mm h^{-1}) mostly occurs in a small area with the number of stations less than 10 % of total weather stations. We have added the following statement at the early part of Sec. 2 in the revised manuscript to describe the background of selecting the threshold values (see also the reply to item (2)). We have also addressed the referee's point about possible dependency of results on the threshold value.

> In order to determine the threshold values for classifying the precipitation types, we have conducted a preliminary statistical analysis on precipitation events in the period of 2011–2015 (not shown). As the precipitation events occur in a given time period and/or space interval, our precipitation data are assumed to follow the Poisson distribution, which represents a probability situation of a large number of observation with a small probability of occurrence. Many studies developed the Poisson distribution models to estimate rainfall and cluster the rainfall systems (e.g., Rodriguez-Iturbe et al., 1987; Lee et al., 2014; Barton et al., 2016; Ritschel et al., 2017). We have chosen the threshold values when the cumulative percentage of precipitation events for each criterion (i.e., C1 and C2) reached approximately 80 %; thus obtaining the threshold values of 20 % for C1 and 3 mm h^{-1} for C2, respectively. Our preliminary statistical analysis showed that, in general, most precipitation events occur over small areas and precipitation events with high intensity rarely occur over large areas. The locality of precipitation appeared higher as the precipitation intensity were higher, in accordance with Nam et al. (2014). In particular, precipitation systems with the highest intensity ($\geq$ 10 mm h^{-1}) were mostly confined to a small area with the number of stations less than 10 % of total weather stations. This implies that the locality feature of precipitation systems may depend on the threshold value in precipitation intensity.

(5) *Page 7, line 22 – Page 8, line 15: The authors need to clearly state how the analyses in this block are related to the "propagation of precipitation systems". Analyses in this block are directly related to spatial structures (e.g., shape and orientation); please explain how can these features be related to "propagation".*

$\Longrightarrow$ We appreciate the referee pointing this out. We noticed that it may cause confusion because the meaning of "propagate" includes "to travel through space" (Merriam-Webster), which entails the concept of time dimension. We actually used the word "propagation" because all the weather systems evolve in time (i.e., develop, mature and decay) and move in space during their life cycles. Furthermore, as we used the 3-year data, the spatial autocorrelations here are considered to include the temporal features implicitly. The fact that precipitation systems have high correlation along a specific direction im-

plies that those systems in that direction, even in far distances, have similar/common structures or are originated from the same weather system. For the meteorological systems with strong directionality, we can mention a squall line or a frontal system in which several thunderstorms banded together, and a multicell cluster that includes a series of individual storm at a different stage of life cycle with the same movement direction. For the multicell cluster, new cells form along the upwind edge of the cluster, and decaying cells are found along the downwind side with mature cells located at the center; thus it includes evolutions in both space and time. We addressed this point in the revised manuscript; nevertheless, we decided to modify the expression "the spatial ***propagation*** of precipitation systems" to "the spatial ***structures*** of precipitation systems" (page 7, line 25), to avoid any confusion.

(6) *The spatial shape differences between the three rainfall types (in the same block as above): the asymmetry indicated in the spatial correlation (Fig. 4) does not correspond well to that depicted in the radar echo (Fig. 5). The directional difference in the* e*-folding scale for the all three systems are about 25% (5km/20km for HPFP; 10km/40km for HPMP and LPMP) of the mean scale (i.e., aspect ratios of ∼1.3) while the radar echoes suggest larger aspect ratios for HPFP and HPMP (∼1). This is not consistent with their interpretation of rainfall system in Page 8, line 10: how often a squall line is of an aspect ratio of 2?*

$\Longrightarrow$ We are not sure if we have fully understood the referee's point/question here. In our understanding, the directional difference of 25 % seems to indicate the ratio of the difference between the largest and the smallest values of the directional e-folding distances (say, Δd) and the largest directional e-folding distance (say, d_{max}), i.e., $\Delta d/d_{max}$. For example, in Fig. 4b, LPMP shows $\Delta d \simeq 10$ km and $d_{max} \simeq 40$ km; thus making the ratio be $\sim 0.25 = 25$ %. It seems that the referee defined the aspect ratio as the largest directional e-folding distance divided by the smallest directional e-folding distance (say, d_{min}), i.e., d_{max}/d_{min}. For example, in Fig. 4b, LPMP shows $d_{max} \simeq 40$ km and $d_{min} \simeq 30$ km; thus making the aspect ratio be ~ 1.3. Probably the referee wanted to mean the aspect ratio of HPFP and HPMP in the radar diagram (Fig. 5) to be ~ 2, not ~ 1.

$\Longrightarrow$ If our understanding above is correct, we make the following reply to the referee's comment. Figure 4 shows the mean directional autocorrelation for different precipitation types, whereas Fig. 5 shows the directional e-folding distance regarding to all cases in each precipitation type by finding the mode in the histogram. Note that the mean e-folding distance (Fig. 4) and the e-folding distance of the mode (Fig. 5) do not necessarily be the same or similar. Although Figs. 4 and 5 are based on the same composite precipitation data, they may be different especially when the deviation of e-folding distance from each case is large. Therefore, they may not match each other for the $e-$folding distances and hence the scales of spatial correlation.

$\Longrightarrow$ Furthermore, please note that the radar diagram (Fig. 5) does not mean the diagram representing radar echoes as the referee mentioned. In other words, Fig. 5 is not related to Fig. 4 in any aspect. To avoid any confusion, we have modified the "radar diagram" to the "radar chart" in the revised manuscript. A *radar chart*, also known as web chart or spider chart, is a graphical method of displaying multivariate data in the form of a two-dimensional chart of three or more quantitative variables represented on axes starting from the same point (source: en.wikipedia.org).

$\Longrightarrow$ We have mentioned that our HPMP case "may" correspond to squall lines as well as convection bands, cloud clusters or the warm-type heavy rainfall, based on the previous studies. However, we have not conducted the analysis for each precipitation type (i.e., squall lines, convection bands, etc.), and hence we do not have any information on the aspect ratio of squall lines in Korea. It is essential to conduct the case studies for each precipitation type in the future.

(7) *Page 8: If the satellite data cannot clearly distinguish the areas of water vapor from those without, how much can we trust the analysis based on the data? Can they provide data quality control of the satellite data?*

$\Longrightarrow$ Satellite images from the water vapor (WV) channels represent several important dynamical features in the upper- and mid-level atmosphere: dry air or clear sky is represented by dark area, moist air or cloudy sky by light area, intrusion of dry air in mature cyclones by dry slot (i.e., dark area), jet stream location by high contrast between dark and light areas (i.e., boundary), upper-level vorticity by rotational patterns of light and dark areas, and so on. In particular, the two WV channels 6.2 and 7.3 μm are sensitive to catch moisture boundaries at the zone between the warm/moist and cold/dry side of the jet/wind maximums at two different levels in the troposphere (Georgiev et al., 2016). Therefore, the satellite data from the WV channels clearly distinguish the dry vs. humid air, and detect the moisture boundary effectively. In the text, we mentioned that it was hard to distinguish between water vapor and clouds, thus used the mixed images. Given that both WV and clouds are the sources of precipitation, analysis of the mixed variables from the satellite data may not make a serious problem in understanding and relating to the precipitation systems. We have rewritten this part in the revised manuscript to deliver our intent more clearly (see the second paragraph of Sec. 4.1.2) as (new sentences in bold):

> In this study, we analyze the brightness temperatures from the Himawari-8 water vapor bands to characterize the lower to upper atmosphere related to the precipitation systems. **A humid atmosphere absorbs more longwave radiation from the Earth, resulting in a lower brightness temperature. On the other hand, a dry atmosphere absorbs less longwave radiation, bringing about a higher brightness temperature. Although we cannot directly quantify the amount of water vapor through the water vapor imager, we can sufficiently recognize the spatial distribution of water vapor. Moreover, using two water vapor channels (i.e., 6.2 and 7.3 μm), we can clearly identify the moisture boundaries at the zone between the warm/moist and cold/dry side of the jet/wind maximums at two different levels in the troposphere (Georgiev et al., 2016).** The spatial analyses were performed with the mixed images of clouds and water vapors **because it was hard to distinguish between clouds and water vapor without a cloud detection algorithm. Since both water vapor and clouds are strongly linked to precipitation as its sources, analysis of the mixed variables from the satellite data would not make a serious problem in understanding and relating to the precipitation systems.** As we focus on the spatial distribution of water vapor when precipitation occurs, we analyze water vapor for each precipitation type.

$\Longrightarrow$ Furthermore, we have added the description of the satellite data quality with new references (i.e., Okuyama et al., 2015) to Sec. 2 as:

> The calibration of the Himawari-8 water vapor bands is accurate to within 0.2 K by validating an approach developed under the Global Space-based Intercalibration System (GSICS) project with hyper-spectral infrared sounders (e.g., Okuyama et al., 2015; Bessho et al., 2016).

(8) *Page 8, line 33: The only similarity between Fig. 2 and Fig. 6 is that the autocorrelation for HPFP decreases more rapidly than those for HPMP and LPMP. The separation between HPFP and HPMP/LPMP in Fig. 6 is much smaller than in Fig. 2 as well. Overall, it's difficult to establish similarity between the spatial scales of water vapor and rainfall. The authors need to provide clear explanations on how to related the structures based on water vapor scales (Fig. 6) to that based on rainfall (Fig. 2). Overall, it is difficult to much merits of the satellite vapor analysis towards the rainfall structure over Korea.*

$\Longrightarrow$ We agree with the referee that it is difficult to establish similarity between the spatial scales of water vapor and rainfall. However, our intent on analyzing the satellite WV data was not only to establish similarity but also to find any possible dissimilarity between WV and precipitation. Since the WV makes phase changes and the conversion from WV to precipitation includes a bunch of nonlinear processes, we did not expect high similarity in the spatial scales and structure between WV and precipitation. Rather, we had scientific curiosity on the degree of similarity vs. dissimilarity, and on what aspects of dissimilarity would be found. As we have focused on the comparison of spatial correlation among precipitation types, we found the similarity between precipitation (Fig. 2) and water vapor (Fig. 6), as mentioned by the referee: the autocorrelation of WV for HPFP decreases more rapidly than those for HPMP and LPMP as in precipitation. We have also found and discussed the dissimilarity, especially on the separation distance, i.e., the spatial scales. We additionally discovered the similarity between WV and precipitation in terms of characteristic directionality in spatial autocorrelations. Through the satellite WV analyses, we also aimed at examining the extent and direction of spatial correlation of WV into the Korean Peninsula in association with the precipitation types. In addition, many studies have been carried out on the relationship between satellite water vapor and extratropical/tropical cyclones and storms (e.g., Velden, 1987; Milford and Dugdale, 1990; Krennert and Zwatz-Meise, 2003; De Haan et al., 2004; Rabin et al., 2004; Mukhopadhyay et al., 2005; Chosh et al., 2008). Further studies on the relationship between precipitation systems and satellite water vapor in Korea are essentially required.

$\Longrightarrow$ We have addressed these points in the revised manuscript. We first modified the first paragraph of Sec. 4.1.2, with new sentences in bold, as:

> Water vapor is the core element and driver of the precipitation development through dynamical processes (e.g., advection and convection) and physical processes (e.g., evaporation and condensation). For example, the East Asian monsoon starts when a huge amount of water vapor from the adjacent ocean is transported to the monsoon region by the large scale atmospheric circulation. Thus, the spatial analysis of water vapor will contribute to further understanding of the spatial patterns of precipitation. **Many studies have been carried out on the relationship between satellite water vapor and extratropical/tropical cyclones and storms (e.g., Velden, 1987; Milford and**

Dugdale, 1990; Krennert and Zwatz-Meise, 2003; De Haan et al., 2004; Rabin et al., 2004; Mukhopadhyay et al., 2005; Chosh et al., 2008).

By analyzing the water vapor imagery, we can detect not only the horizontal distribution of tropospheric water vapor but also the dynamical behavior of atmospheric flow such as the middle and upper troughs, vortexes, and jet streams, even in the absence of clouds. Therefore, analyzing the spatial characteristics of tropospheric water vapor is essential to improve the understanding of precipitation systems. **In particular, we are focusing on the extent and direction of spatial correlation of water vapor into the Korean Peninsula in association with the precipitation types.**

$\Longrightarrow$ We have also added the following paragraph to the end of Sec. 4.1.2:

Through the satellite water vapor analyses, we found both similarity and dissimilarity in spatial correlations between water vapor and precipitation. Similar to the results of precipitation analyses, the spatial autocorrelations of water vapor for HPFP decreased more rapidly than those for HPMP and LPMP (cf. Figs. 2 and 6). Water vapor and precipitation showed additional similarity in terms of characteristic directionality in spatial autocorrelations (cf. Figs. 4 and 7, and Figs. 5 and 8). However, both fields showed significant dissimilarity in the separation distances, i.e., the spatial scales (cf. Figs. 2 and 6). Note that water vapor makes phase changes and the conversion from water vapor to precipitation includes a bunch of nonlinear processes; thus it is not surprising to see such dissimilarity. Further studies on the relationship between precipitation systems and satellite water vapor in Korea are essentially required.

(9) *Temporal correlation analysis: It's not clear what we can learn about the rainfall systems from the temporal correlation characteristics. The e-folding scale differs by only 30 mins among the three types. The time scale of 1–1.5 hours seem to indicate that the all three rainfall types are related to convective systems, either isolated or clustered. Does this provide any insights to separate the characteristics of the three rainfall types? Also, it's not clear how the water vapor analysis can be related to the rainfall characteristics.*

$\Longrightarrow$ We appreciate the referee pointing this issue out. We agree with the referee that the e-folding time is in the range of 1–2 hours and there is no significant difference by precipitation types. Nevertheless, we believe that this finding has some meaningful implications. First, as the referee has pointed out, the relatively short e-folding time scale for all precipitation types implies that the precipitation systems affecting Korea in summer are mostly characterized by convective-type precipitation, from either isolated storm cells or clustered bands, at least for the analysis period. Second, the e-folding time scale suggests a proper time interval for data collection and analysis for capturing the detailed structure of and better forecasting of precipitation systems. Lastly, it has another important implication on data assimilation, especially on the proper time interval of incorporating observations in the operational data assimilation system, for more accurate numerical forecasting of the precipitation systems. We also note that a similar result was reported by Ha et al. (2007), showing the e-folding time of precipitation in Korea is 1–2 hours regardless of months (i.e., May to September). Therefore, we can conclude that the typical e-folding time of the precipitation systems in Korea is 1–2 hours, regardless of

the precipitation types. This conclusion is based on the analyses of the hourly precipitation data: we may find different temporal characteristics for different precipitation types using a data set of shorter interval (e.g., 10 min). A further work is also necessary to investigate the relationship between water vapor transport and precipitation, regarding the temporal scale as well as the spatial scale, with more detailed analyses. We have addressed these points in the revised manuscript by adding the following two paragraphs to the end of Sec. 4.3:

> Through this temporal correlation analyses, we noticed that the e-folding time is in a short range (1–2 hours), and its difference among different precipitation types is only about 30 min. This short e-folding time scale for all precipitation types implies that the precipitation systems affecting Korea in summer are mostly characterized by convective-type precipitation, from either isolated storm cells or clustered bands, at least for the given analysis period. The e-folding time scale suggests an adequate time interval for data collection and analysis for capturing the detailed structure of and better forecasting of precipitation systems. It also implies a proper time interval of incorporating observations in the operational data assimilation system, for more accurate numerical forecasting of the precipitation systems.
>
> Moreover, Ha et al. (2007) reported that the e-folding time of precipitation in Korea is 1–2 h regardless of months (from May to September), and that the monthly difference of the e-folding time is approximately 30–40 min. Therefore, we can conclude that the typical e-folding time of the summer precipitation systems in Korea is 1–2 h, regardless of the precipitation types and months. This conclusion is based on the analyses of the hourly precipitation data: we may find different temporal characteristics for different precipitation types using a data set of shorter interval (e.g., 10 min). In terms of the satellite water vapor data, a further study is also necessary to investigate the relationship between water vapor transport and precipitation, regarding the temporal scale as well as the spatial scale, with more detailed analyses.

(10) *Considering the aspect ratio and spatial scales, the examples in Fig. 11 seem more relevant for convective clusters (may be imbedded within a frontal structure) than a frontal system.*

$\Longrightarrow$ As Fig. 11 depicts an HPFP case in October, we agree with the referee's opinion that the case seems to be related to convective clusters. In Section 4.1.1, we also mentioned that HPFP may correspond to the isolated thunderstorms or convection bands as well as frontal rainfalls. To avoid confusion, we have rewritten the statement in page 10, line 25 as:

> "For example, precipitation in the HPFP case**, relevant to convective clusters,** appeared over a small local area (Fig. 11a) but the value of global Moran's I was much higher (0.2357) than the others (0.1207 and 0.1711), implying a stronger cluster pattern; however, considering that the global Moran's I is a domain-averaged value, this high value may be due to less dispersion (negative correlation) areas."

Table R1. Preliminary statistical analysis of precipitation events during 2011–2015 by two criteria – the portion of weather stations with precipitation and the station average precipitation rate. The red lines indicate the boundaries when the cumulative percentage of precipitation events is approximately 80 %.

		The portion of weather stations with precipitation (%)												
		0-10	10-20	20-30	30-40	40-50	50-60	60-70	70-80	80-90	90-	Sum	Percentage (%)	Cumulative percentage (%)
The station average precipitation rate (mm/h)	0.1-0.9	5241	399	156	60	29	5	2	1	0	0	5893	40.0	40.0
	1.0-1.9	2238	665	383	235	148	99	57	33	18	6	3882	26.3	66.3
	2.0-2.9	891	352	262	196	109	89	48	35	29	12	2023	13.7	80.0
	3.0-4.9	765	322	224	212	159	85	77	43	49	35	1971	13.4	93.3
	5.0-9.9	317	118	116	115	76	47	35	19	18	8	869	5.9	99.2
	10.0-	61	6	19	11	14	1	0	0	0	0	112	0.8	100.0
	Sum	9513	1862	1160	829	535	326	219	131	114	61	14750		
	Percentage (%)	64.5	12.6	7.9	5.6	3.6	2.2	1.5	0.9	0.8	0.4			
	Cumulative percentage (%)	64.5	77.1	85.0	90.6	94.2	96.4	97.9	98.8	99.6	100.0			

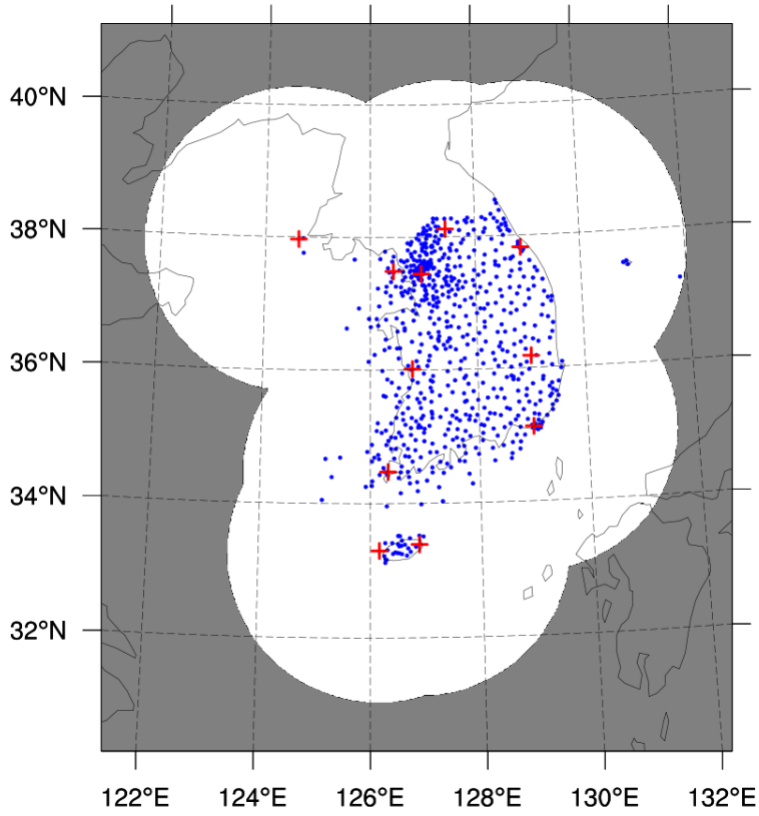

Figure R1. The weather station locations (blue dots) and radar locations (red "+" symbols) and coverages (white area) in Korea.

References

Barton, Y., Giannakaki, P., Von Waldow, H., Chevalier, C., Pfahl, S., and Martius, O.: Clustering of regional-scale extreme precipitation events in Southern Switzerland, Mon. Wea. Rev., 144, 347–369, 2016.

Bessho, K., Date, K., Hayashi, M., Ikeda, A., Imai, T., Inoue, H., ⋯, and Yoshida, R.: An introduction to Himawari-8/9 — Japan's new-generation geostationary meteorological satellites, J. Meteorol. Soc. Japan Ser. II, 94, 151–183, 2016.

Choi, S.-W., Lee, S.-J., Kim, J. Lee, B.-L., Kim, K.-R., and Choi, B.-C.: Agrometeorological observation environment and periodic report of Korea Meteorological Administration: Current status and suggestions, Korean J. Agric. For. Meteorol., 17, 144–155, doi:10.5532/KJAFM.2015.17.2.144, 2015 (in Korean with English abstract).

Chosh, A., Lohar, D., and Das, J.: Initiation of Nor'wester in relation to mid-upper and low-level water vapor patterns on METEOSAT-5 images, Atmos. Res., 87, 116–135, 2008.

De Haan, S., Barlag, S., Baltink, H. K., Debie, F., and Van der Marel, H.: Synergetic use of GPS water vapor and Meteosat images for synoptic weather forecasting, J. Appl. Meteor., 43, 514–518, 2004.

Georgiev, C. G., Santurette, P., and Maynard K.: Weather Analysis and Forecasting: Applying Satellite Water Vapor Imagery and Potential Vorticity Analysis, 2nd Ed., Academic Press, Cambridge, USA, 2016.

Krennert, T. and Zwatz-Meise, V.: Initiation of convective cells in relation to water vapour boundaries in satellite images, Atmos. Res., 67–68, 353–366, 2003.

Lee, J., Yoon, J., and Jun, H. D.: Evaluation for the correction of radar rainfall due to the spatial distribution of raingauge network, J. Korea Soc. Hazard Mitig., 14, 337–345, http://dx.doi.org/10.9798/KOSHAM.2014.14.6.337, 2014 (in Korean with English abstract).

Milford, J.R. and Dugdale, G.: Estimation of rainfall using geostationary satellite data, in: Applications of Remote Sensing in Agriculture, Steven, M. D. and Clark, J. A., Eds., Butterworth, 97–110, 1990.

Mukhopadhyay, P., Singh, H. A. K., and Singh, S. S.: Two severe Nor'westers in April 2003 over Kolkata using Doppler Radar observations and satellite imagery, Weather, 60, 343–353, 2005.

Nam, J.-E., Lee, Y. H., Ha, J.-C., and Cho, C.-H.: A study on the e-folding distance of summer precipitation using precipitation reanalysis data, in: Proc. the Autumn Meeting of Korean Meteorological Society, 2014, Korean Meteorol. Soc., Jeju, Korea, 13–15 October 2014, 657–658, 2014.

Okuyama, A., Andou, A., Date, K., Hosaka, K., Mori, N., Murata, H., Tabata, T., Takahashi, M., Yoshino, R. and Bessho, K.: Preliminary validation of Himawari-8/AHI navigation and calibration, Proc. SPIE 9607, Earth Observing Systems XX, 96072E, doi:10.1117/12.2188978, 2015.

Rabin, R. M., Corfidi, S. F., Brunner, J. C., and Hane, C. E.: Detecting winds aloft from water vapor satellite imagery in the vicinity of storms, Weather, 59, 251–257, doi:10.1256/wea.182.03, 2004.

Ritschel, C., Ulbrich, U., Névir, P., and Rust, H. W.: Precipitation extremes on multiple timescales — Bartlett-Lewis rectangular pulse model and intensity-duration-frequency curves, Hydrol. Earth Syst. Sci., 21, 6501–6517, https://doi.org/10.5194/hess-21-6501-2017, 2017.

Rodriguez-Iturbe, I., Cox, D. R., and Isham, V.: Some models for rainfall based on stochastic point processes, Proc. R. Soc. London, Ser. A, 410, 269–288, 1987.

Velden, C. S.: Satellite observations of Hurricane Elena (1985) using the VAS 6.7 μm "water-vapor" channel, Bull. Amer. Meteor. Soc., 68, 210–215, 1987.

Geostatistical assessment of ~~summertime rainfall~~ warm-season precipitation observations in Korea based on the composite precipitation and satellite water vapor data

Sojung Park[1,3,4], Seon Ki Park[1,2,3,4], Jeung Whan Lee[5], and Yunho Park[5]

[1]Department of Climate and Energy Systems Engineering, Ewha Womans University, Seoul, Republic of Korea
[2]Department of Environmental Science and Engineering, Ewha Womans University, Seoul, Republic of Korea
[3]Severe Storm Research Center, Ewha Womans University, Seoul, Republic of Korea
[4]Center for Climate/Environment Change Prediction Research, Ewha Womans University, Seoul, Republic of Korea
[5]Korea Meteorological Administration, Seoul, Republic of Korea

Correspondence: S. K. Park (spark@ewha.ac.kr)

Abstract. Among the meteorological disasters, heavy rainfalls cause the second largest damage in Korea, following typhoons. To confront with the potential disasters due to heavy rainfalls, understanding the observational characteristics of precipitation is of utmost importance. In this study, we investigate the spatial and temporal characteristics of ~~summertime~~ warm-season precipitation in Korea, according to the precipitation types, by conducting the geostatistical analyses such as autocorrelogram, Moran's I and general G, on the composite (radar ~~+~~ + station) precipitation data. The e-~~folding~~ -folding distance of precipitation ranges from 15 to 35 km, depending on the spatial distribution, rather than intensity, of precipitation, whereas the e-~~folding~~ -folding time ranges from 1 to 2 h. The directional analyses revealed that the ~~summertime precipitation~~ warm-season precipitation systems in Korea, especially those with high precipitation amount, have high spatial autocorrelations in ~~Korea has high spatial correlations in~~ the southwest–northeast and west–east directions, ~~mainly due to frontal rainfallsduring the monsoon season.~~ in association with the frontal rainfalls, convection bands, etc. Furthermore, the cluster versus dispersion patterns and the hot versus cold spots are analyzed through Moran's I and general G, respectively. Water vapor, represented by the brightness temperature, from three Himawari-8 water vapor bands also show similar characteristics with precipitation but with strong spatial correlation over much longer distance (∼100 km), possibly due to the continuity of water vapor. We found that, under the e-~~folding-based~~ -folding based standard, the current observation network of Korea is sufficient to capture the characteristics of most precipitation systems; however, under a strict standard (e.g., autocorrelation of 0.6), a higher-resolution observation network is essentially required — especially in local areas with frequent heavy rainfalls — depending on the directional features of precipitation systems. Establishing such an observation network based on the characteristics of precipitation enables us to improve monitoring/tracking/prediction skills of high-impact weather phenomena as well as to enhance the utilization of numerical weather prediction.

1 Introduction

Heavy rainfall causes one of the most serious meteorological disasters in Korea. Most precipitation systems in Korea are highly influenced by the East Asian summer monsoon, called *Changma* in Korean (Riyu et al., 2001; Kim et al., 2002; Lee et al., 2017b), and hence have high seasonal variation~~:~~; they also show high spatial variation due to complex topographic features (e.g., Ko et al., 2005; Chang and Kwon, 2007; Park and Lee, 2007; In et al., 2014). Since heavy rainfalls including typhoon cause serious damages to both human life and property, improving the their forecast accuracy is of utmost importance. Many studies have been done to improve the quantitative precipitation forecast using numerical weather prediction models and satellite or radar data (e.g., Fritsch et al., 1998; Lee et al., 2006; Kim and Oh, 2010; Yerong and David, 2006; Yu et al., 2013). In order to improve the forecast accuracy, it is essential to understand the spatial and temporal characteristics as well as the occurrence and development mechanisms of the precipitation systems.

The ground-based rainfall observation data, in Korea, are collected from ~~both~~ the Automated Synoptic Observing Systems (ASOS)~~and~~ , the Automatic Weather Stations (AWS), and the Automated Agriculture Observing System (AAOS). The observation density is about 67 km for ASOS and approximately 13 km by including AWS. The agrometeorological observation network consists of 11 AAOS stations (Choi et al., 2015). Based on these precipitation observations, the mesoscale structures of precipitation as well as the hydrologic budgets in Korea have been extensively studied (e.g., Kim and Lee, 2006; Cassardo et al., 2009; Jeong et al., 2012; 2016; Jung and Lee, 2013; Lee et al., 2017a). Capturing the ~~characteristic~~ spatiotemporal features of precipitation systems ~~out of~~ from the observation networks is essential to runoff forecast, especially at the catchment scale and for the flooding cases ~~, for accurate and reliable spatiotemporal estimates of precipitation are crucial to the successful forecast of catchment response~~ (Volkmann et al., 2010). Given the limited resources, it is desirable to optimally design the observation networks, which should be efficient to use the least amount of available instruments but sufficient to capture the precipitation characteristics — both amount and spatiotemporal variability. In other words, understanding temporal and spatial characteristics of precipitation is fundamental and essentially required for establishment of the optimal observation networks (see Ciach and Krajewski, 2006; Volkmann et al., 2010). ~~However~~Moreover, the appropriateness of such observation networks, in analyzing and/or forecasting the precipitation systems, has seldom been assessed.

In this study, we investigate the spatial and temporal characteristics of precipitation in Korea using the geostatistical analysis methods — autocorrelogram, Moran's I, and general G (e.g., Ciach and Krajewski, 2006; Schiemann et al., 2011; Emmanuel et al., 2012; Fu et al., 2014). Ciach and Krajewski (2006) estimated the spatial correlation functions in small-scale rainfall, based on raingauges covering an area of about 3 km by 3 km in Central Oklahoma. They showed a dependence of the correlogram parameters on the averaging time scale, large differences of the correlograms in the individual storms, and the ambiguities in correlation estimates based on rainfall intensities. Bacchi and Kottegoda (1995) addressed the effects of weather systems, topography, and temporal/spatial scale of observation networks on spatial distribution of rainfall. Emmanuel et al. (2012) analyzed the characteristics of spatiotemporal variability by rainfall ~~type~~ types using variogram.

In Korea, the spatial and temporal characteristics of precipitation have been reported in several previous studies (e.g., Chang and Kwon, 2005; Hong et al., 2006; Ha et al., 2007; In et al., 2014). Ha et al. (2007) found that the e ~~-folding~~ -folding distance

and time in correlation coefficients of AWS precipitation ranged from 50 to 110 km and 1 to 2 h, respectively. In summer, precipitation showed localized features with relatively more precipitation mainly in the western part and southern coastal areas of Korea (Kim et al, 2005; Hong et al., 2006; In et al. 2014). In et al. (2014) also analyzed the degree of localization in summer precipitation, and noted a high locality of rainfalls, i.e., more frequent occurrence of short-lived local precipitation, in July and August. In addition to these studies, we provide further analyses on variation of spatial correlation associated with distribution and intensity of precipitation.

Water vapor is also strongly linked to the precipitation system because not only it is the absolute source of precipitation (Eltahir and Bras, 1996; Park, 1999; Bretherton et al., 2004; Stohl et al., 2008; Gimeno et al., 2012) but also its transport in the lower troposphere provides diabatic heating and hence promotes development of convective precipitation systems (Tompkins, 2001; Trenberth and Stepaniak, 2003a, b; Smith and Yuter, 2010). Therefore, the amount and behavior of water vapor are the crucial factors in the precipitation system. For instance, a large amount of water vapor originated from the adjacent oceans is transported to the East Asian monsoon region through the large scale monsoon circulations. The origins of water vapor supply can also distinguish the anomalous rainfall patterns (e.g., Zhou and Yu, 2005). Furthermore, about 70 % of precipitation in extratropical cyclones is generated by water vapor already present when the storm formed in the atmosphere (Trenberth, 1999). Hence, we also conduct the spatial and temporal analysis of water vapor to enhance the understanding of precipitation characteristics over Korea and adjacent areas.

This study aims at classifying the precipitation types statistically based on the spatial distribution of precipitation, and identifying the spatial and temporal characteristics of ~~summertime~~ warm-season precipitation in Korea according to the precipitation types via the geostatistical analysis methods, including autocorrelogram, Moran's I, and general G. Furthermore, we investigate the characteristics of water vapor over the Korean Peninsula associated with the precipitation types, using satellite data. Section 2 describes the data set used for the analyses, and Sect. 3 briefly introduces the geostatistical methods employed in this study. Results and discussions are provided in Sect. 4. Section 5 is devoted to conclusions.

2 Data description

~~The Korea Meteorological Administration (KMA) has produced a composite precipitation data over Korea based on the radar data, from which non-precipitation echoes were removed using the satellite cloud type data. Then the radar data were corrected by and combined with the AWS data of about 600 stations (Hwang et al. , 2015). This data covers 1153 km × 1441 km over the Korean Peninsula, with a grid size of~~ We use the precipitation data from weather stations (see Fig. 1~~km and a time resolution of 1 h. Geostatistical analyses are conducted using this precipitation data sets from April to October in a period of 2013–2015 to investigate the spatial and temporal characteristics of summer rainfall.~~) to categorize the precipitation systems. We classify four different precipitation types statistically, based on two criteria: the portion of weather stations with precipitation (C1; in %), and the station average precipitation rate (C2; in mm h^{-1}). In order to determine the threshold values for classifying the precipitation types, we have conducted a preliminary statistical analysis on precipitation events in the period of 2011–2015 (not shown). As the precipitation events occur in a given time period and

space interval, our precipitation data are assumed to follow the Poisson distribution, which represents a probability situation of a large number of observation with a small probability of occurrence. Many studies developed the Poisson distribution models to estimate rainfall and to cluster the rainfall systems (e.g., Rodriguez-Iturbe et al., 1987; Lee et al., 2014; Barton et al., 2016; Ritschel et al., 2017). We have chosen the threshold values when the cumulative percentage of precipitation events for each criterion (i.e., C1 and C2) reached approximately 80 %; thus obtaining the threshold values of 20 % for C1 and 3 mm h^{-1} for C2, respectively. Our preliminary statistical analysis showed that, in general, most precipitation events occur over small areas and precipitation events with high intensity rarely occur over large areas. The locality of precipitation appeared higher as the precipitation intensity were higher, in accordance with Nam et al. (2014). In particular, precipitation systems with the highest intensity ($\geq$ 10 mm h^{-1}) were mostly confined to a small area with the number of stations less than 10 % of total weather stations. This implies that the locality feature of precipitation systems may depend on the threshold value in precipitation intensity.

Based on these criteria, we define four different precipitation types, as shown in Table 1: 1) Low Precipitation at a Few Points (LPFP) for C1 $<$ 20 % and C2 $<$ 3 mm h^{-1}; 2) Low Precipitation at Many Points (LPMP) for C1 $\geq$ 20 % and C2 $<$ 3 mm h^{-1}; 3) High Precipitation at a Few Points (HPFP) for C1 $<$ 20 % and C2 $\geq$ 3 mm h^{-1}; and 4) High Precipitation at Many Points (HPMP) for C1 $\geq$ 20 % and C2 $\geq$ 3 mm h^{-1}. We practically exclude the LPFP type in our analyses, i.e., the case with C1 $<$ 20 % and C2 $<$ 3 mm h^{-1}, for it may be less effective.

The Korea Meteorological Administration (KMA) has produced the composite precipitation data over Korea using the data from radars, weather stations and satellites, through the following steps (see Hwang et al., 2015): 1) remove non-precipitation echoes from the radar data using the satellite cloud type data; 2) calculate the difference between the station precipitation and the radar estimated precipitation; 3) perform the objective analysis on the precipitation difference field and on the station precipitation data; 4) correct the bias using the objectively-analyzed difference field; and 5) combine the corrected radar-estimated precipitation data and the objectively-analyzed station precipitation data to produce the composite precipitation data (in mm h^{-1}). In order to analyze the precipitation systems with the evenly distributed high-resolution data, we used these composite precipitation data, which cover 1153 km $\times$ 1441 km over the Korean Peninsula, with a grid size of 1 km and a time resolution of 1 h. Geostatistical analyses are conducted using the composite precipitation data sets from April to October in a period of 2013–2015 to investigate the spatial and temporal characteristics of warm-season rainfall.

We also used the Himawari-8 water vapor bands to investigate the distribution feature of water vapor in the lower to upper atmosphere in association with precipitation. The water vapor bands are strongly linked with the properties of moisture, thermodynamics and dynamics of the troposphere. As they are sensitive to the moisture and temperature profiles in the radiation path, they can provide information for a wide range of atmospheric processes (Georgiev et al., 2016), including atmospheric motions such as the upper-level lows, jet stream, and blocking. Himawari-8, operated by the Japan Meteorological Agency since 7 July 2015, carries a new unit called the Advanced Himawari Imager (AHI) with higher radiometric, spectral, and spatial resolution in the geostationary orbit (Bessho et al., 2016). The AHI has 16 observation bands — three visible (0.47, 0.51, 0.64 μm), three near-infrared (0.86, 1.6, 2.3 μm), and ten infrared (3.9, 6.2, 6.9, 7.3, 8.6, 9.6, 10.4, 11.2, 12.4, 13.3 μm). Among them the water vapor absorption bands — 8 (6.2 μm), 9 (6.9 μm), and 10 (7.3 μm) — represent upper-, mid-, and

mid-/lower-level water vapor, respectively. The calibration of the Himawari-8 water vapor bands ~~are strongly linked with the properties of moisture, thermodynamics and dynamics of the troposphere.As they are sensitive to the moisture and temperature profiles in the radiation path, they can provide information for a wide range of atmospheric processes (Georgiev~~ is accurate to within 0.2 K by validating an approach developed under the Global Space-based Intercalibration System (GSICS) project with hyper-spectral infrared sounders (e.g., Okuyama et al., 2015; Bessho et al., 2016)~~, including atmospheric motions such as the upper-level lows, jet stream, and blocking~~. In this study, we used the scan area for Full Disk by AHI that covers the East Asia region: the Full Disk images are taken every 10 min with a 2 km spatial resolution. The analyses are conducted on the data of the hour over the domain of 120.132−134.243°E and 30.436−44.068°N (600 × 770 grids), similar to the area of the precipitation data.

3 Geostatistical methods

In this study, we use several methods to analyze the spatial characteristics — the spatial autocorrelation, Moran's I, and general G. The spatial autocorrelation shows how the precipitation observations at a certain distance are correlated with each other. Thus, it is possible to determine the degree of spatial scale, or the effective influence range, of a single precipitation system or associated precipitation systems. Through Moran's I, we can figure out the property of spatial correlations, especially distinguishing between the cluster and dispersion patterns/areas of precipitation. In other words, Moran's I identifies local cluster areas of strong precipitation, large areas of precipitation, or precipitation boundaries. General G indicates whether the cluster region has high or low precipitation.

3.1 Spatial autocorrelation

Autocorrelation in spatial analysis implies that a variable is correlated with itself at different points. Simply speaking, pairs of precipitation data close to each other likely to have more similar values than those far apart from each other. When the precipitation data are spatially autocorrelated, precipitation at one place is related to that at another place, and they are not independent to each other. The autocorrelation coefficient can be obtained once the autocovariance has been calculated. The autocovariance indicates the degree of similarity of a variable itself at a certain distance. Generally, the autocovariance is greater as the separation distance decreases, becomes smaller as the distance increases, and does not show any tendency (e.g., converge) after a certain distance. For the one-dimensional data, the autocovariance (cov) in terms of the grid distance (or lag; k) between the data pairs, $X = (x_1, x_2, \cdots, x_{n-k})$ and $X' = (x_{1+k}, x_{2+k}, \cdots, x_n)$, is defined as:

$$\begin{aligned} cov(X, X') &= E[(X - \mu_X)(X' - \mu_{X'})] \\ &= E(XX') - E(X)E(X') \\ &= \mu_{XX'} - \mu_X \mu_{X'}. \end{aligned} \tag{1}$$

Here $E(XX')$, $E(X)$ and $E(X')$ are the means of sub-datasets (i.e., XX', X and X', respectively), and are calculated as the followings:

$$E(XX') = \frac{1}{n-k}\sum_{i=1}^{n-k} x_i x_{i+k} = \mu_{XX'}, \quad (2)$$

$$E(X) = \frac{1}{n-k}\sum_{i=1}^{n-k} x_i = \mu_X$$

and

$$E(X') = \frac{1}{n-k}\sum_{i=1}^{n-k} x_{i+k} = \mu_{X'},$$

where n is the number of total points and i is the grid point index. The lag index, k, depicts the grid distance between two point values, x_i and x_{i+k}. The autocorrelation coefficient (ρ) is defined as:

$$\rho(X,X') = \frac{cov(X,X')}{\sqrt{var(X)var(X')}} = \frac{\mu_{XX'} - \mu_X\mu_{X'}}{\sqrt{var(X)var(X')}}, \quad (3)$$

where $var(X)$ means the variance of X and can be regarded as the covariance of X with itself, i.e., $var(X) = cov(X,X)$. At the zero separation distance, the autocovariance has the same value as the variance and the autocorrelation coefficient becomes unity. For the two-dimensional data, the autocorrelation coefficient of all data pairs within the separation distance is obtained by using the relaxed separation distance, and by following the same calculation principle as in the one-dimensional data. In order to compute the relaxed separation distance, the distance between the data pairs is rounded.

3.2 Moran's *I*

Moran's I is a statistical index for measuring the similarity of neighboring data (Moran, 1948). It is obtained by comparing the values of the target and neighboring feature pairs with the average of the entire targets:

$$I = \frac{n\sum_i\sum_j w_{ij}(x_i-\overline{x})(x_j-\overline{x})}{\sum_i\sum_j w_{ij}\sum_i(x_i-\overline{x})^2}, \quad (4)$$

where n is the number of the entire target observations, x_i is the variable value at the i-th location, $\overline{x}$ is the mean of the entire targets. Here, w_{ij} is the spatial weight of the link between i and j, which is defined by the inverse distance weight, i.e., $w_{ij} = 1/d_{ij}$ with d_{ij} representing the distance between grids i and j. Moran's I is ranged from -1 to 1 with the following interpretation: 1) the positive value means that the variable of interest and its spatial lags are positively autocorrelated, defining a *cluster* pattern; 2) the negative value indicates spatially negative autocorrelation, defining a *dispersion* pattern; and 3) the zero value represents a *random* spatial pattern. Equation (4) denotes the global Moran's I that identifies the pattern — either cluster or dispersion — but with no information on the magnitude of variables. In addition, the local Moran's I (I_i), showing the location of cluster/dispersion, is computed as the following (Anselin, 1995):

$$I_i = \frac{(x_i-\overline{x})}{\sum_{k=1}^{n}(x_k-\overline{x})^2/(n-1)}\sum_{j=1}^{n} w_{ij}(x_j-\overline{x}). \quad (5)$$

I_i is interpreted the same as I but with no specific range. The Z-score (Z) can be analyzed together to confirm the significance of I_i, and is calculated as:

$$Z(I_i) = \frac{I_i - E(I_i)}{SD(I_i)}, \tag{6}$$

where $E(I_i) = -\sum_j w_{ij}/(n-1)$ is the expected value of I_i if random, and $SD(I_i)$ is the standard deviation of I_i. The Z-score suggests whether we can reject the null hypothesis or not. In this case, the null hypothesis states "there is no spatial clustering". To determine if the Z-score is statistically significant, we compare it to the range of values for a particular confidence level. For example, at the significance level of 0.1, 0.05, 0.01, the absolute value of Z-score would have to be greater than 1.65, 1.96, 2.57, respectively, to be statistically significant, and the clusters are not created by chance.

3.3 General *G*

We can identify the cluster patterns through Moran's I; however, it does not indicate whether the clustered variable values are low or high. In addition to Moran's I, it is necessary to determine whether the properties of the cluster are hot spots (i.e., high values) or cold spots (i.e., low values) by using Getis-Ord general G (Getis and Ord, 1992; hereafter, referred to as general G). The global general G, like the global Moran's I, shows the cluster characteristics for the entire study area as a statistical index. Therefore, we use the local general G which can represent locations where features with either high or low values are spatially clustered. The following equation calculates the local general G ($G_i(d)$):

$$G_i(d) = \frac{\sum_j w_{ij}(d)x_j}{\sum_j x_j}, \quad j \neq i, \tag{7}$$

where d is the distance between the target feature and the neighboring feature, and w_{ij} is the same spatial weight (i.e., the inverse distance weight) used for calculating Moran's I as in Eqs. (4) and (5). To be a statistically significant hot spot or cold spot, the Z-score of general G can be calculated. Ord and Getis (1995) redefined $G_i(d)$, which can be considered as the Z-score ($Z(G_i)$), as:

$$Z(G_i) = \frac{G_i - E(G_i)}{SD(G_i)}, \quad j \neq i, \tag{8}$$

where $E(G_i) = \sum_j w_{ij}(d)/(n-1)$ is the expected value if random, and $SD(G_i)$ is the standard deviation of G_i. High positive values indicate the possibility of a local cluster of high values, whereas negative values indicate a similar cluster of low values. An absolute value of the Z-score would have to be greater than 1.65, 1.96, 2.57 to be statistically significant at a significance level of 0.1, 0.05, 0.01, respectively.

4 Results and discussions

4.1 Spatial autocorrelation

4.1.1 Precipitation

The general characteristics of the spatial autocorrelation structure in precipitation for each type are shown in Fig. 2. We have calculated the correlation coefficients for all points in the range from 0 to 100 km. In order to compare the characteristics between different precipitation types, we defined the e-folding value as the threshold. The e-folding distance means the separation distance when autocorrelation becomes e^{-1} (i.e., 0.3674). In other words, it refers to the spatial scale of precipitation that autocorrelation decreases to $\rho = e^{-1}$ from the value at the zero separation distance (i.e., $\rho = 1$). The e-folding value, under the assumption that atmospheric variables decrease exponentially with time and distance, has often been used to estimate both the temporal and spatial structure of precipitation (e.g., Skøien et al, 2003; Ha et al., 2007; Kursinski and Mullen, 2008; Zeweldi and Gebremichael, 2009; In et al., 2014). As classified in Table 1, the LPMP and HPMP cases (i.e., C1 is high, regardless of C2) show the e-folding distance at ∼35 km. On the other hand, the HPFP cases (i.e., C1 is low) depict the e-folding distance at ∼15 km.

This result can be expected from the classification of precipitation types: precipitation with smaller spatial scale brings about more rapid decrease in the spatial correlation, thus showing smaller correlation at the e-folding distance. Ha et al. (2007) estimated the e-folding distance of summertime folding distance of warm-season precipitation as 50–110 km, and In et al. (2014) pointed out that the e-folding distance varied depending on months and regions with the minimum being 40 km. Our results show shorter e-folding distances than those from the previous studies: it is ascribed to exclusion of the LPFP cases (see Table 1). Nam et al. (2014) examined the relationship between precipitation intensity and spatial autocorrelation, and noticed that the latter became smaller as the former appeared stronger, thus depicting a larger locality in precipitation. They found that the e-folding distance was 14 km for the precipitation intensity in excess of 30 mm h^{-1}, whereas it was about 40 km for the intensity greater than 5 mm h^{-1}. However, our results indicate that the spatial autocorrelations of HPMP and LPMP are in similar shape. Generally, the spatial locality is proportional to precipitation intensity; however, strictly speaking, the number of points with precipitation has a greater effect on spatial characteristics than the precipitation intensity.

In Fig. 3, in order to identify the spatial characteristics of precipitation for each case, we show a histogram depicting the number of cases according to the e-folding distance. We found that the e-folding distance of the mode (the most frequent value) was 15 km for HPFP, 30 km for LPMP, and 34.7 km for HPMP, respectively. It is evident that, as shown in Fig. 2, the e-folding distance depends on the precipitation spatial scale rather than the precipitation intensity.

We additionally analyzed the directional features of precipitation distribution over the Korean Peninsula in order to know the spatial propagation structures of precipitation systems (see Figs. 4 and 5). We classified the direction range from 0° to 180° with an interval of 45°, considering the symmetry. Here the direction is a measure of the angle from the origin–east axis, whose magnitude increases counterclockwise (see the radar diagram chart in Fig. 5). Figure 4 shows the averaged directional

autocorrelation for different precipitation types. The autocorrelation curves show similar shape and property in HPMP (Fig. ~~4a~~ 4a) and HPFP (Fig. 4c), which depict two distinct directional characteristics: the precipitation structures have similar spatial features in directional pair of 45° and 0° and of 135° and 90°. For HPFP where the precipitation spatial scale is small, the autocorrelations of all directions decrease more rapidly than those for LPMP and HPMP, resulting in a smaller gap between the two distinct curves compared to HPMP. For LPMP, i.e., low precipitation rate with a large spatial scale, the spatial correlation is the highest with the precipitation axis of 45° (i.e., ~~southwest-northeast~~southwest–northeast), whereas it is the lowest with that of 135° (~~northwest-southeast~~northwest–southeast).

Figure 5 shows a radar ~~diagram~~ chart representing the directional e ~~-folding~~ -folding distance at the mode in the directional histogram of case numbers (not shown). In general, the directional e ~~-folding~~ -folding distances (and hence the spatial correlations) are larger for the cases with large spatial scale (i.e., LPMP and HPMP) than the cases with small spatial scale (i.e., HPFP). It is noteworthy that the e ~~-folding~~ -folding distances in LPMP have no characteristic directionality (i.e., isotropic), indicating that the precipitation systems in LPMP ~~move in various directions~~ are mostly related to both the migratory cyclones that move into Korea from various directions and the cloud clusters where moderate convective systems in large area are closely connected to each other. On the other hand, the cases with high precipitation intensity, i.e., HPFP and HPMP, both show strong directionality (i.e., anisotropic) with large e ~~-folding~~ -folding distances along the axes of 45~~°~~ ° and 0~~°~~ ° (i.e., the ~~southwest-northeast and west-east~~ southwest–northeast and west–east directions, respectively). ~~These~~ They are considered to be strongly linked to the frontal rainfalls, convection bands, etc. (e.g., Sun and Lee, 2002; Kim and Lee, 2006; Lee et al., 2008; Jeong et al., 2012, 2016; Jung and Lee, 2013).

As we have used the 3-year data, the spatial autocorrelations here are considered to include the temporal features implicitly. All the weather systems evolve in time (i.e., develop, mature and decay) and move in space during their life cycles. The fact that precipitation systems have high correlation along a specific direction implies that those systems in that direction, even in the far distances, have similar/common structures or are originated from the same weather system. For instance, the meteorological systems with strong directionality include a squall line or a frontal system in which several thunderstorms banded together, and a multicell cluster that comprises a series of individual storm at a different stage of life cycle with the same movement direction. For the multicell cluster, new cells form along the upwind edge of the cluster, and decaying cells are found along the downwind side with mature cells located at the center; thus it includes evolutions in both space and time.

In terms of the summertime heavy precipitation systems over the Korean Peninsula, Lee and Kim (2007) classified them into four major types such as isolated thunderstorms, convection bands, squall lines and cloud clusters, whereas Song and Sohn (2015) classified them into two types: the cold type characterized by an eastward moving cloud system with an oval shape, and the warm type with a comparatively wide spatial distribution over an area extending from the southwest to northeast. In our case, the precipitation events in HPFP may correspond to the isolated thunderstorms or the cold-type heavy rainfalls while those in HPMP to convection bands, squall lines, cloud clusters or the warm-type heavy rainfalls. On the other hand, Ha et al. (2007) investigated the monthly characteristics in the directional features of rainfall from May to September, and reported that the cell type was dominant in May and September while the ~~southwest-northeast~~ southwest–northeast tilted band type was ruling in June–August. They addressed that the band type is mainly due to frontal rainfall during the rainy season. In our results,

most cases of HPMP and HPFP occurred in July and August (see Table 2); thus, indicating that ~~their precipitation systems are~~ the warm-season precipitation systems in Ha et al. (2007) are mostly related to the long-lived (HPMP) and short-lived (HPFP) band type heavy rainfalls along the monsoon frontal system.

4.1.2 Himawari-8 water vapor bands

Water vapor is the core element and driver of the precipitation development through dynamical processes (e.g., advection and convection) and physical processes (e.g., evaporation and condensation). For example, the East Asian monsoon starts when a huge amount of water vapor from the adjacent ocean is transported to the monsoon region by the large scale atmospheric circulation. Thus, the spatial analysis of water vapor will contribute to further understanding of the spatial patterns of precipitation. Many studies have been carried out on the relationship between satellite water vapor and extratropical/tropical cyclones and storms (e.g., Velden, 1987; Milford and Dugdale, 1990; Krennert and Zwatz-Meise, 2003; De Haan et al., 2004; Rabin et al., 2004; Mukhopadhyay et al., 2005; Chosh et al., 2008).

By analyzing the water vapor imagery, we can detect not only the horizontal distribution of tropospheric water vapor but also the dynamical behavior of atmospheric flow such as the middle and upper troughs, vortexes, and jet streams, even in the absence of clouds. Therefore, analyzing the spatial characteristics of tropospheric water vapor is essential to improve the understanding of precipitation systems. In particular, we are focusing on the extent and direction of spatial correlation of water vapor flowing into the Korean Peninsula in association with the precipitation types.

In this study, we analyze the brightness temperatures from the Himawari-8 water vapor bands to characterize the lower to upper atmosphere related to the precipitation systems. ~~Here,~~ A humid atmosphere absorbs more longwave radiation from the Earth, resulting in a lower brightness temperature~~means that the top of moisture layer is located at a higher altitude and hence contains more water vapor . It is not possible to distinguish between clouds and water vapors without a cloud detection algorithm, thus the~~ . On the other hand, a dry atmosphere absorbs less longwave radiation, bringing about a higher brightness temperature. Although we cannot directly quantify the amount of water vapor through the water vapor imager, we can sufficiently recognize the spatial distribution of water vapor. Moreover, using two water vapor channels (i.e., 6.2 and 7.3 μm), we can clearly identify the moisture boundaries at the zone between the warm/moist and cold/dry side of the jet/wind maximums at two different levels in the troposphere (Georgiev et al., 2016). The spatial analyses were performed with the mixed images of clouds and water ~~vapors. In the analyses of water vapor bands, it should be noted that the brightness temperature cannot clearly distinguish between the areas with and without water~~ vapor because it was hard to distinguish between clouds and water vapor without a cloud detection algorithm. Since both water vapor and clouds are strongly linked to precipitation as its sources, analysis of the mixed variables from the satellite data would not make a serious problem in understanding and relating to the precipitation systems. As we focus on the spatial distribution of water vapor when precipitation occurs, we analyze water vapor for each precipitation type.

The general characteristics of the spatial autocorrelation structure in water vapor bands for each precipitation type are shown in Fig. 6. The patterns of spatial autocorrelations of water vapor bands, for three precipitation types, are generally similar to those of precipitation; however, the separation distances extend much longer (cf. Fig. 2). Even at a separation distance of

100 km, the spatial correlation is higher than 0.6. This strong spatial correlation is considered to be due to the continuity of water vapor. The largest spatial autocorrelation appears in LPMP, followed by HPMP and HPFP. The LPMP depicts similar correlation coefficients regardless of bands and hence heights of atmospheric layers. This implies that the spatial structure of water vapor bands is similar in the vertical. On the other hand, the spatial correlations in HPMP and HPFP become smaller along the downward path, from band 8 to band 10.

In Fig. 7, the brightness temperature of water vapor bands characterizes directionality in the spatial correlations. In general, for all precipitation types and water vapor bands, the highest spatial correlations appear in the axis of 45° (southwest-northeast) while the lowest in the axis of 135° (northwest-southeast), as in precipitation (cf. Fig. 4). In LPMP, the spatial correlations in the axes of 0° and 90° coincide even at longer distances. We also notice that, for a given precipitation type and separation distance, the spatial autocorrelation of water vapor becomes larger along the upward path, from band 10 to band 8. Figure 8 shows the directional separation distances at the mode in the directional histogram of case numbers (not shown) for each precipitation type with the autocorrelation coefficients of 0.7 (blue), 0.8 (black), and 0.9 (grey), respectively. The separation distances generally show high values mainly in the axis of 45°, similar to the directional features of precipitation (cf. Fig. 5). Note that, in LPMP, the brightness temperature shows a large separation distance (i.e., high spatial correlation) in the axis of 45° ~~(i.e., band type)~~ while precipitation depicts no directionality (~~i.e., cell type;~~ cf. Fig. 5). This is possible because water vapor can form as a band type, e.g., over a stationary front but precipitation can occur in cell type due to local features of convection over the same front. In addition, as the autocorrelation coefficient decreases, the directionality tends to disappear even though the autocorrelation coefficient is as large as 0.7. As in Fig. 7, we note that for a given precipitation type and spatial autocorrelation, the separation distance of water vapor becomes larger along the upward path. This is related to the stronger wind at upper atmosphere that carries the characteristic feature of water vapor further downstream.

Through the satellite water vapor analyses, we found both similarity and dissimilarity in spatial correlations between water vapor and precipitation. Similar to the results of precipitation analyses, the spatial autocorrelations of water vapor for HPFP decreased more rapidly than those for HPMP and LPMP (cf. Figs. 2 and 6). Water vapor and precipitation showed additional similarity in terms of characteristic directionality in spatial autocorrelations (cf. Figs. 4 and 7, and Figs. 5 and 8). However, both fields showed significant dissimilarity in the separation distances, i.e., the spatial scales (cf. Figs. 2 and 6). Note that water vapor makes phase changes and the conversion from water vapor to precipitation includes a bunch of nonlinear processes; thus it is not surprising to see such dissimilarity. Further studies on the relationship between precipitation systems and satellite water vapor in Korea are essentially required.

4.2 Moran's I and general G

Moran's I represents the spatial distribution pattern, i.e., cluster or dispersion: the cluster (dispersion) patterns appear in the areas with positive (negative) spatial autocorrelation. General G determines whether the cluster area is a hot or cold spot: a hot (cold) spot means an area with high (low) values and hence high (low) precipitation amount. For all precipitation cases in this study, the values of global Moran's I showed positive values meaning that clusters were detected, in the domain-average sense. Through the local Moran's I (I_i), we can define the similarity between the target feature and its neighbors, and check the spatial

outliers as well (Lalor and Zhang, 2001; McGrath and Zhang, 2003). For example, with a negative I_i, the target feature may have high precipitation while its surroundings have low precipitation, and vice versa. Conversely, with a positive I_i, the target feature has similar amount of precipitation as its neighbors. Thus, the local Moran's I can detect strong precipitation over local clusters, precipitation boundaries, or precipitation over large areas. As Moran's I cannot distinguish between low and high precipitation, we employed the local general G to identify the hot/cold spots (i.e., high/low precipitation areas, respectively). In order to calculate the indices, we selected a sub-domain for each precipitation case where the precipitation values were extracted at an interval of 5 km. An inverse distance weighting function is used as the spatial weight.

We present the analysis results for three cases — one from each precipitation type (see Figs. 9–11). For the selected cases, the values of global Moran's I were all positive: 0.1207, 0.1711 and 0.2357 for the cases of LPMP, HPMP and HPFP, respectively, with a higher value representing a stronger clustering. This indicates that all three cases show the cluster patterns. Figure 9 shows an LPMP case, occurred at 05 Korean Standard Time (KST) 25 August 2015, in association with a tropical cyclone. Typhoon Goni (2015) approached from Japan and brought rainfall all over Korea (Fig. 9a). In particular, heavy precipitation systems, with more than 30 mm h^{-1}, developed around the mountain range along the east-central coast of the Korean Peninsula. In Fig. 9b, the southeastern region is identified as hot spots (areas of high precipitation) while the southwestern region, over both land and sea, as cold spots (areas of low precipitation). Figure 9c depicts ~~development of several single-cell storms with maximum precipitation rate~~ several precipitation systems with maximum intensity (i.e., precipitation rate; see Fig. 9a) in the cluster area (marked by the ~~crosses).~~ X symbols). These systems show the highest local Moran's I with the spatial scale of less than 30 km. The cluster patterns were statistically significant at a significance level of 0.01 (Fig. 9d). In Fig. 10, we illustrate a heavy rainfall case in the category of HPMP, which occurred at 17 KST 27 May 2013 as a migratory cyclone approached from the west, passed over the Korean Peninsula slowly, and brought rainfall throughout the country, mainly in the western and southern regions (Fig. 10a). Such precipitation areas matched well with the hot spots in Fig. 10b. The map of local Moran's I shows that a ~~strong cluster~~ precipitation system with a strong cluster feature has developed, over the southwestern sea of the Korean Peninsula, along with the successive cluster patterns in a line type (Fig. 10c), with a significance level of 0.01 (Fig. 10d). Figure 11 shows an HPFP case, occurred at 05 KST 24 October 2015. The central-western region of the Korean Peninsula received rainfall of more than 8 mm h^{-1} (Fig. 11a): the hot spots appeared in the precipitation area while the cold spots were located at the region of relatively low precipitation (Fig. 11b). Figure 11c illustrates an intense cluster pattern (dark red) over the relatively high rainfall area, and a weaker cluster pattern over the cold spot, with a significance level of about 0.01 (Fig. 11d).

Overall, the spatial structures of the selected precipitation systems are well presented by the analyses of Moran's I and general G. The overall spatial pattern (cluster vs. dispersion) of a precipitation system is characterized by the global Moran's I, whereas the spatial distributions of clustered areas are represented by the local Moran's I. The overall regional features of precipitation amount (i.e., hot vs. cold spot) are captured by the local general G. For example, precipitation in the HPFP case, relevant to convective clusters, appeared over a small local area (Fig. 11a) but the value of global Moran's I was much higher (0.2357) than the others (0.1207 and 0.1711), implying a stronger cluster pattern; however, considering that the global Moran's I is a domain-averaged value, this high value may be due to less dispersion (negative correlation) areas. In fact, the

HPFP case shows a relatively weaker dispersion area (Fig. 11c), compared to the LPMP and HPMP cases (Figs. 9c and 10c, respectively). It is notable that the cluster pattern shows different spatial characteristics depending on the spatial scale and distribution feature of precipitation systems: several strong local clusters develop, especially over areas of high precipitation, when precipitation occurs over a large region (Figs. 9 and 10), whereas weaker clusters develop when precipitation occurs over a small region (Fig. 11). Through the integrated interpretation of these indices, we discovered some important spatial features of the precipitation systems: 1) the area where the cluster pattern overlaps with the hot spots is characterized by heavy rainfall (e.g., the ~~X-marked~~ X-marked or dark red places in Figs. 9c and 10c); 2) the area where the dispersion pattern concurs with the cold spots is distinguished by a relatively high precipitation surrounded by low precipitation (e.g., the rain cells denoted by arrows in Figs. 9c and 10c); 3) the precipitation gets weaker as it moves away from the strong cluster area, that is, the cluster pattern appears at the center and the dispersion pattern appears around; and 4) the secondary cluster pattern in a precipitation system over a wide area indicates clusters of low-intensity precipitation.

4.3 Temporal autocorrelation

We additionally calculated the temporal autocorrelation ~~coefficient~~ coefficients of precipitation and water vapor bands for each precipitation type. For precipitation, HPFP represents the shortest e~~-folding~~ -folding time, followed by LPMP and HPMP (Fig. 12). This order in the e~~-folding~~ -folding time is the same as in the e~~-folding~~ -folding distance: this implies that, for the precipitation types classified here, the spatial correlation as well as the temporal correlation appears greater in the precipitation systems over a larger area than those over a smaller area. The range of the e~~-folding~~ -folding time for all precipitation types is 1–2 hours. The averaged temporal autocorrelations of water vapor bands show similar features to those of precipitation for different precipitation types, though the correlations decrease slowly over time (Fig. 13). In addition, compared with the spatial correlations, the temporal correlations do not show significant dependence on the height of atmospheric layer.

Through this temporal correlation analyses, we noticed that the e-folding time is in a short range (1–2 hours), and its difference among different precipitation types is only about 30 min. This short e-folding time scale for all precipitation types implies that the precipitation systems affecting Korea in the warm season are mostly characterized by convective-type precipitation, from either isolated storm cells or clustered bands, at least for the given analysis period. The e-folding time scale suggests an adequate time interval for data collection and analysis for capturing the detailed structure of and better forecasting of precipitation systems. It also implies a proper time interval of incorporating observations in the operational data assimilation system, for more accurate numerical forecasting of the precipitation systems.

Moreover, Ha et al. (2007) reported that the e-folding time of precipitation in Korea is 1–2 h regardless of months (from May to September), and that the monthly difference of the e-folding time is approximately 30–40 min. Therefore, we can conclude that the typical e-folding time of the warm-season precipitation systems in Korea is 1–2 h, regardless of the precipitation types and months. This conclusion is based on the analyses of the hourly precipitation data: we may find different temporal characteristics for different precipitation types using a data set of shorter interval (e.g., 10 min). In terms of the satellite water vapor data, a further study is also necessary to investigate the relationship between water vapor transport and precipitation, regarding the temporal scale as well as the spatial scale, with more detailed analyses.

5 Conclusions

Heavy rainfall causes many casualties as well as property damage, and thus its accurate forecast is very important. To improve the forecast accuracy, it is necessary to understand the characteristics of the precipitation systems through analyses of data from observation and/or numerical modeling. Furthermore, a well-designed observation network is essentially required to capture the characteristic features of precipitation systems.

In this study, we ~~assess the current observational network~~ identify the characteristics of warm-season precipitation systems in Korea, ~~focusing on the summertime heavy precipitation systems,~~ via the geostatistical analyses on the composite precipitation and satellite water vapor data. We have classified the precipitation cases into four types, based on the average rainfall amount per point and the ratio of the points with precipitation (i.e., spatial scale): 1) Low Precipitation at a Few Points (LPFP); 2) Low Precipitation at Many Points (LPMP); 3) High Precipitation at a Few Points (HPFP); and 4) High Precipitation at Many Points (HPMP), among which the LPFP cases are excluded from the analysis.

We have conducted analyses of the spatial and temporal autocorrelations of precipitation and water vapor for the precipitation cases of each classification type, and found that the e~~–folding~~ -folding distance of precipitation ranges between 15 and 35 km while the e~~–folding~~ -folding time ranges between 1 and 2 h. The e~~–folding~~ -folding distance is as short as 15 km for an HPFP case (e.g., a local shower), but as large as 35 km for the cases of both LPMP and HPMP, implying that the spatial correlation becomes larger as precipitation occurs over a wider area and is less affected by the precipitation amount. We also noted that the spatial ~~autocorrelation has characteristic directionality :~~ autocorrelations have characteristic directionality as the followings: 1) precipitation systems with ~~large~~ high precipitation amount (i.e., HPFP and HPMP) have high spatial ~~correlation in the southwest-northeast and west-east~~ autocorrelations in the southwest–northeast and west–east directions, mainly ~~due to frontal rainfall~~ associated with frontal rainfalls during the monsoon season~~.~~; and 2) those with low precipitation amount (i.e., LPMP) have no directionality, pertaining to both the migratory cyclones moving in various directions and the moderate convective systems in the cloud clusters. Other spatial characteristics were identified as well, including cluster ~~vs.~~ versus dispersion patterns, hot ~~vs.~~ versus cold spots, strong precipitation over local clusters, precipitation boundaries, precipitation over a large area, ~~etc~~and so forth. In general, heavy rainfalls appear over the hot spots with the cluster pattern while an isolated high precipitation system, surrounded by low precipitation, occurs over the cold spots with the dispersion pattern.

The Advanced Himawari Imager (AHI), on board Himawari-8, has three water vapor bands — 8 (6.2 μm), 9 (6.9 μm) and 10 (7.3 μm) — representing lower atmospheric layer with higher wavelength. Since water vapor has continuity in time and space, the autocorrelation coefficients of water vapor bands drop more slowly than the composite precipitation. However, the comparative analyses according to the precipitation type reveal that the spatial correlations of water vapor bands behave similarly to those of precipitation: the correlations of water vapor bands are also large (small) for precipitation systems occurred over a large (small) area.

~~Currently, Korea has~~ We can also assess the current observational network in Korea, focusing on the warm-season precipitation systems, via the geostatistical analyses. Currently, the precipitation observation network ~~with~~ in Korea has a spatial resolution of ~13 km, distributing the analysis in an interval of 1 h. For a standard based on the e~~–folding~~ -folding values, such observa-

tion network is capable of deriving the spatiotemporal characteristics of the precipitation systems in all three types — LPMP, HPMP and HPFP. However, if we apply a strict standard (e.g., autocorrelation of 0.6), the separation distance and time for the HPFP cases fall down to ∼6 km and ∼35 min, respectively. This implies that~~the~~ , regarding the spatial resolution, the current observation network can hardly capture the characteristic features of the localized ~~heavy rainfall systemswith the current spatial resolution: the~~ precipitation systems; the temporal resolution might be sufficiently high because the composite precipitation data are produced at every 10 min. Therefore, for more accurate analyses of the precipitation systems with a higher correlation, a denser observation network should be considered in local areas where a heavy rainfall often occurs. This study has enabled us not only to explore the characteristics of ~~the~~ precipitation systems in Korea but also to suggest the criteria for evaluating the observation network.

We note that the spatial distribution and movement features of the precipitation systems are strongly affected by terrain, but the orographic effect is not fully assessed in this study. Bacchi and Kottegoda (1995) demonstrated the orographic effect of the Alps mountain range on the spatial distribution of the rainfalls and addressed the directional characteristics of the spatial correlations. Other studies also confirmed the direct and induced effect of mountain on spatial distribution of rainfall (e.g., Mass, 1981; Carruthers and Choularton, 1983; Barros and Kuligowski, 1997; ~~Mass, 1981;~~ Park and Lee, 2007). As the Korean Peninsula is represented by a highly complex terrain with many mountains, the spatial properties of precipitation systems will be distinctively affected. It is essential to conduct a further research about the orographic effect on the spatiotemporal characteristics of precipitation, specifically over different slope sides of various mountain ranges in Korea. We additionally suggest a further study to analyze the autocorrelations by considering the storm cell movement and the occurrences of initial precipitation and maximum rainfall intensity.

Data availability. The composite precipitation and Himawari-8 data are available from the Korea Meteorological Administration database: http://203.247.66.28/ (instructed in Korean), in which a user registration is required. The Himawari-8 data is also disseminated via the HimawariCast from the Japan Meteorological Agency at http://www.data.jma.go.jp/mscweb/en/himawari89/himawari_cast/himawari_cast.html.

Acknowledgements. This work is supported by the Korea Meteorological Administration (KMA) Research and Development Program under Grant KMIPA, mainly through KMIPA2016-1010 and partly through KMI2018-06710. We acknowledge KMA for supplying the composite precipitation and the Himawari-8 water vapor bands data.

References

Anselin, L.: Local Indicators of Spatial Association — LISA, Geogr. Anal., 27, 93–115, doi: 10.1111/j.1538-4632.1995.tb00338.x, 1995.

Bacchi, B. and Kottegoda, N. T.: Identification and calibration of spatial correlation patterns of rainfall, J. Hydrol., 165, 311–348, 1995.

Barros, A. P. and Kuligowski, R.J.: Orographic effects during a severe wintertime rainstorm in the Appalachian mountain, Mon. ~~Weather~~ Wea. Rev., 126, 2648–2672, 1997.

Barton, Y., Giannakaki, P., Von Waldow, H., Chevalier, C., Pfahl, S., and Martius, O.: Clustering of regional-scale extreme precipitation events in southern Switzerland, Mon. Wea. Rev., 144, 347–369, 2016.

Bessho, K., Date, K., Hayashi, M., Ikeda, A., Imai, T., Inoue, H., Kumagai, Y., Miyakawa, T., Murata, H., Ohno, T., Okuyama, A., Oyama, R., Sasaki, Y., Shimazu, Y., Shimoji, K., Sumida, Y., Suzuki, M., Taniguchi, H., Tsuchiyama, H., Uesawa, D., Yokota, H., and Yoshida, R.: An introduction to Himawari-8/9 — Japan's new-generation geostationary meteorological satellites, J. Meteorol. Soc. Japan Ser. II, 94, 151–183, 2016.

Bretherton, C. S., Peters, M. E., Back, L. E.: Relationships between water vapor path and precipitation over the tropical oceans, J. Clim., 17, 1517–1528, doi: 10.1175/1520-0442(2004)017<1517:RBWVPA>2.0.CO;2, 2004.

Carruthers, D.J. and Choularton, T.W.: A model of the feeder-seeder mechanism of orographic rain including stratification and wind-drift effects, Quart. J. R. Meteorol. Soc., 109, 575–588, 1983.

Cassardo, C., Park, S. K., Thakuri, B. M., Priolo, D., and Zhang, Y.: Soil surface energy and water budgets during a monsoon season in Korea, J. Hydrometeor., 10, 1379–1396, 2009.

~~Carruthers, D.J. and Choularton, T.W.: A model of the feeder-seeder mechanism of orographic rain including stratification and wind-drift effects, Quart. J. R. Meteorol. Soc., 109, 575–588, 1983.~~

Chang, H. and Kwon, W.-T.: Spatial variations of summer precipitation trends in South Korea, 1973–2005, Environ. Res. Lett., 2, 045012, doi:10.1088/1748-9326/2/4/045012, 2007.

Ciach, G. J. and Krajewski, W. F.: Analysis and modeling of spatial correlation structure in small-scale rainfall in Central Oklahoma, Adv. Water Resour., 29, 1450–1463, 2006.

Choi, S.-W., Lee, S.-J., Kim, J. Lee, B.-L., Kim, K.-R., and Choi, B.-C.: Agrometeorological observation environment and periodic report of Korea Meteorological Administration: Current status and suggestions, Korean J. Agric. For. Meteorol., 17, 144–155, doi:10.5532/KJAFM.2015.17.2.144, 2015 (in Korean with English abstract).

Chosh, A., Lohar, D., and Das, J.: Initiation of Nor'wester in relation to mid-upper and low-level water vapor patterns on METEOSAT-5 images, Atmos. Res., 87, 116–135, 2008.

De Haan, S., Barlag, S., Baltink, H. K., Debie, F., and Van der Marel, H.: Synergetic use of GPS water vapor and Meteosat images for synoptic weather forecasting, J. Appl. Meteor., 43, 514–518, 2004.

Eltahir, E. A. B. and Bras, R. L.: Precipitation recycling, Rev. Geophys., 34, 367–378, doi: 10.1029/96RG01927, 1996.

Emmanuel, I., Andrieu, H., Leblois, E., and Flahaut, B.: Temporal and spatial variability of rainfall at the urban hydrological scale, J. Hydrol., 430, 162–172, 2012.

Fritsch, J. M., Houze Jr. R. A., Adler, R., Bluestein, H., Bosart, L., Brown, J., Carr, F., Davis, C., Johnson, R. H., Junker, N., Kuo, Y.-H., Rutledge, S., Smith, J., Toth, Z., Wilson, J. W., Zipser, E., and Zrnic, D.: Quantitative precipitation forecasting: Report of the eighth prospectus development team, U.S. Weather Research Program~~.~~, B. Am. Meteorol. Soc., 79, 285–299, 1998.

Fu, W. J., Jiang, P. K., Zhou, G. M., and Zhao, K. L.: Using Moran's I and GIS to study the spatial pattern of forest litter carbon density in a subtropical region of southeastern China, Biogeosci., 11, 2401–2409, https://doi.org/10.5194/bg-11-2401-2014, 2014.

Georgiev, C. G., Santurette, P., and Maynard K.: Weather Analysis and Forecasting: Applying Satellite Water Vapor Imagery and Potential Vorticity Analysis, 2nd Ed., Academic Press, Cambridge, USA, 2016.

Getis, A. and Ord, J. K.: The analysis of spatial association by use of distance statistics, Geogr. Anal., 24, 189–206, 1992.

Gimeno, L., Stohl, A., Trigo, R. M., Dominguez, F., Yoshimura, K., Yu, L., Drumond, A., Durán-Quesada, A. M., and Nieto, R.: Oceanic and terrestrial sources of continental precipitation, Rev. Geophys., 50, RG4003, doi:10.1029/2012RG000389, 2012.

Ha, K.-J., Jeon, E.-H., and Oh, H.-M.: Spatial and temporal characteristics of precipitation using an extensive network of ground gauge in the Korean Peninsula, Atmos. Res., 86, 330–339, 2007.

Hong, K.-O., Shu, M.-S., and Rha, D.-K.: Temporal and spatial variations of precipitation in South Korea for recent 30 Years (1976–2005) and geographic environments, J. Korean Earth Sci. Soc., 27, 433–449, 2006 (in Korean with English abstract).

Hwang, D.-I., Lee, J. W., Seo, D.-I., Na, H., and Seo, Y.-K.: Prediction system using extrapolation-based nowcasting techniques for very short-range forecasting and improvement of 1 hr accumulated precipitation forecasts, in: Proceedings of the Autumn Meeting of Korean Meteorological Society, 2015, Jeju, Korea, 12–14 October 2015, 260–261, 2015.

In, S.-R., Han, S.-O.,Im, E.-S.,Kim, K.-H., and Shim, J.: Study on temporal and spatial characteristics of summertime precipitation over Korean Peninsula, Atmos., 24, 159–171, 2014.

Jeong, J.-H., Lee, D.-I., Wang, C.-C., Jang, S.-M., You, C.-H., and Jang, M.: Environment and morphology of mesoscale convective systems associated with the Changma front during 9–10 July 2007, Ann. Geophys., 30, 1235–1248, https://doi.org/10.5194/angeo-30-1235-2012, 2012.

Jeong, J.-H., Lee, D.-I., Wang, C.-C., and Han, I.-S.: Characteristics of mesoscale-convective-system-produced extreme rainfall over south-eastern South Korea: 7 July 2009, Nat. Hazards Earth Syst. Sci., 16, 927–939, https://doi.org/10.5194/nhess-16-927-2016, 2016.

Jung, W. and Lee, T.-Y.: Formation and evolution of mesoscale convective systems that brought the heavy rainfall over Seoul on September 21, 2010, Asia-Pacific J. Atmos. Sci., 49, 635–647, doi: 10.1007/s13143-013-0056-4, 2013.

Kim, B. J., Kripalani, R., Oh, J. H., and Moon, S.-E.: Summer monsoon rainfall patterns over South Korea and associated circulation features, Theor. Appl. Climatol. 72, 65–74, doi: 10.1007/s007040200013, 2002.

Kim, E.-H., Kim, M.-K., and Lee, W.-S.: The regional characteristics of daily precipitation intensity in Korea for recent 30 years, J. Korean Earth Sci. Soc., 26, 404–416, 2005 (in Korean with English abstract).

Kim, H. W. and Lee, D. K.: An observational study of mesoscale convective systems with heavy rainfall over the Korean Peninsula, Wea. Forecasting, 21, 125–148, doi: 10.1175/WAF912.1, 2006.

Kim, O. Y. and Oh, J. H.: Verification of the Performance of the High Resolution QPF Model for Heavy Rainfall Event over the Korean Peninsula, Asia-Pacific J. Atmos. Sci., 46, 119–133, 2010.

Ko, J.-W., Baek, H.-J., and Kwon, W.-T.: The characteristics of precipitation and regionalization during rainy season in Korea, J. Korean Meteorol. Soc., 41, 101–114, 2005 (in Korean with English abstract).

Krennert, T. and Zwatz-Meise, V.: Initiation of convective cells in relation to water vapour boundaries in satellite images, Atmos. Res., 67–68, 353–366, 2003.

Kursinski, A. L. and Mullen, S. L.: Spatiotemporal variability of hourly precipitation over the eastern contiguous United States from stage IV multisensor analyses, J. Hydrometeor., 9, 3–21, 2008.

Lalor, G. and Zhang, C.S.: Multivariate outlier detection and remediation in geochemical databases, Sci. Total Environ., 281, 99–109, 2001.

Lee, D.-K., Park, J.-G., and Kim, J.-W.: Heavy Rainfall Events Lasting 18 Days from July 31 to August 17, 1998, over Korea, J. Meteorol. Soc. Japan, Ser. II, 86, 313–333, doi: 10.2151/jmsj.86.313, 2008.

Lee, J., Yoon, J., and Jun, H. D.: Evaluation for the correction of radar rainfall due to the spatial distribution of raingauge network, J. Korea Soc. Hazard Mitig., 14, 337–345, http://dx.doi.org/10.9798/KOSHAM.2014.14.6.337, 2014 (in Korean with English abstract).

Lee, J.-Y., Kim, W., and Lee, T.-Y.: Physical and dynamic factors that drove the heavy rainfall event over the middle Korean Peninsula on 26-27 July 2011, Asia-Pacific J. Atmos. Sci., 53, 101—120, https://doi.org/10.1007/s13143-017-0009-4, 2017a.

Lee, J.-Y., Kwon, M., Yun, K.-S., Min, S.-K., Park, I.-H., Ham, Y.-G., Jin, E. K., Kim, J.-H., Seo, K.-H., Kim, W., Yim, S.-Y., and Yoon, J.-H.: The long-term variability of Changma in the East Asian summer monsoon system: A review and revisit, Asia-Pacific J. Atmos. Sci., 53, 257–272, https://doi.org/10.1007/s13143-017-0032-5, 2017b.

Lee, T.-Y. and Kim, Y.-H.: Heavy precipitation systems over the Korean Peninsula and their classification, J. Korean Meteorol. Soc., 43, 367–396, 2007.

Lee, Y. H., Park, S. K., and Chang, D.-E.: Parameter estimation using the genetic algorithm and its impact on quantitative precipitation forecast, Ann. Geophys., 24, 3185–3189, https://doi.org/10.5194/angeo-24-3185-2006, 2006.

Mass, C.: Topographically forced convergence in western Washington State, Mon. Wea. Rev., 109, 1335–1347, 1981.

McGrath, D. and Zhang, C.: Spatial distribution of soil organic carbon concentrations in grassland of Ireland, Appl. Geochem., 18, 1629–1639, 2003.

Milford, J.R. and Dugdale, G.: Estimation of rainfall using geostationary satellite data, in: Applications of Remote Sensing in Agriculture, Steven, M. D. and Clark, J. A., Eds., Butterworth, 97–110, 1990.

Moran, P. A. P.: The interpretation of statistical maps, J. Roy. Stat. Soc. B. Met., 10, 243–251, 1948.

Mukhopadhyay, P., Singh, H. A. K., and Singh, S. S.: Two severe Nor'westers in April 2003 over Kolkata using Doppler Radar observations and satellite imagery, Weather, 60, 343–353, 2005.

Nam, J.-E., Lee, Y. H., Ha, J.-C., and Cho, C.-H.: A study on the e-folding distance of summer precipitation using precipitation reanalysis data, in: ~~Proceedings of~~ Proc. the Autumn Meeting of Korean Meteorological Society, 2014, Korean Meteorol. Soc., Jeju, Korea, 13–15 October 2014, 657–658, 2014.

Okuyama, A., Andou, A., Date, K., Hosaka, K., Mori, N., Murata, H., Tabata, T., Takahashi, M., Yoshino, R. and Bessho, K.: Preliminary validation of Himawari-8/AHI navigation and calibration. Proc. SPIE 9607, Earth Observing Systems XX, 96072E, doi:10.1117/12.2188978, 2015.

Ord, J. K. and Getis, A.: Local spatial autocorrelation statistics: distributional issues and an application, Geogr. Anal., 27, 286–306, 1995.

Park, S. K.: Nonlinearity and predictability of convective rainfall associated with water vapor perturbations in a numerically simulated storm, J. Geophys. Res., 104(D24), 31575–31587, doi:10.1029/1999JD900446, 1999.

Park, S. K. and Lee, E.: Synoptic features of orographically enhanced heavy rainfall on the east coast of Korea associated with Typhoon Rusa (2002), Geophys. Res. Lett., 34, L02803, doi:10.1029/2006GL028592, 2007.

Rabin, R. M., Corfidi, S. F., Brunner, J. C., and Hane, C. E.: Detecting winds aloft from water vapor satellite imagery in the vicinity of storms, Weather, 59, 251–257, doi:10.1256/wea.182.03, 2004.

Ritschel, C., Ulbrich, U., Névir, P., and Rust, H. W.: Precipitation extremes on multiple timescales—Bartlett-Lewis rectangular pulse model and intensity-duration-frequency curves, Hydrol. Earth Syst. Sci., 21, 6501–6517, https://doi.org/10.5194/hess-21-6501-2017, 2017.

Riyu, L., Oh, J. H., Kim, B. J., Baek, H.-J., and Ronghui, H.: Associations with the interannual variations of onset and withdrawal of the Changma, Adv. Atmos. Sci., 18, 1066–1080, https://doi.org/10.1007/s00376-001-0023-3, 2001.

Rodriguez-Iturbe, I., Cox, D. R., and Isham, V.: Some models for rainfall based on stochastic point processes, Proc. R. Soc. London, Ser. A, 410, 269–288, 1987.

Schiemann, R., Erdin, R., Willi, M., Frei, C., Berenguer, M., and Sempere-Torres, D.: Geostatistical radar-raingauge combination with nonparametric correlograms: methodological considerations and application in Switzerland, Hydrol. Earth Syst. Sci., 15, 1515–1536, https://doi.org/10.5194/hess-15-1515-2011, 2011.

Sherwood, S. C., Roca, R., Weckwerth, T. M., and Andronova, N. G.: Tropospheric water vapor, convection, and climate, Rev. Geophys., 48, RG2001, doi:10.1029/2009RG000301, 2010.

~~Smith, B. L. and Yuter, S. E.: Water vapor fluxes and orographic precipitation over northern California associated with a landfalling atmospheric river, Mon. Wea. Rev. 138, 74–100, doi: 10.1175/2009MWR2939.1, 2010.~~

Skøien, J. O., Blöschl, G., and Western, A. W.: Characteristic space scales and timescales in hydrology, Water Resour. Res., 39, 1304, doi:10.1029/2002WR001736, 2003.

Smith, B. L. and Yuter, S. E.: Water vapor fluxes and orographic precipitation over northern California associated with a landfalling atmospheric river, Mon. Wea. Rev. 138, 74–100, doi: 10.1175/2009MWR2939.1, 2010.

Song, H.-J. and Sohn, B.-J.: Two heavy rainfall types over the Korean Peninsula in the humid East Asian summer environment: A satellite observation study, Mon. Wea. Rev., 143, 363–382, doi: 10.1175/MWR-D-14-00184.1, 2015.

Stohl, A., Forster, C., and Sodemann, H.: Remote sources of water vapor forming precipitation on the Norwegian west coast at 60°N – a tale of hurricanes and an atmospheric river, J. Geophys. Res., 113, D05102, doi:10.1029/2007JD009006, 2008.

Sun, J. and Lee, T.-Y.: A Numerical Study of an Intense Quasi-stationary Convection Band over the Korean Peninsula, J. Meteorol. Soc. Japan, Ser. II, 80, 1221–1245, doi: 10.2151/jmsj.80.1221, 2002.

Tompkins, A. M.: Organization of tropical convection in low vertical wind shears: The role of water vapor, 58, 529–545, doi: 10.1175/1520-0469(2001)058<0529:OOTCIL>2.0.CO;2, 2001.

Trenberth, K. E.: Atmospheric moisture recycling: Role of advection and local evaporation, J. Clim., 12, 1368–1381, 1999.

Trenberth, K. E. and Stepaniak, D. P.: Co-variability of components of poleward atmospheric energy transports on seasonal and interannual timescales, J. Clim., 16, 3690–3704, 2003a.

Trenberth, K. E. and Stepaniak, D. P.: Seamless poleward atmospheric energy transports and implications for the Hadley circulation, J. Clim., 16, 3705–3721, 2003b.

Velden, C. S.: Satellite observations of Hurricane Elena (1985) using the VAS 6.7 μm "watervapor" channel, B. Am. Meteorol. Soc., 68, 210–215, 1987.

Volkmann, T. H. M., Lyon, S. W., Gupta, H. V., and Troch, P. A.: Multicriteria design of rain gauge networks for flash flood prediction in semiarid catchments with complex terrain, Water Resour. Res., 46, W11554, doi:10.1029/2010WR009145, 2010.

Yerong, F. and Kitzmiller, D. H.: A short-range quantitative precipitation forecast algorithm using back-propagation neural network approach, Adv. Atmos. Sci., 23, 405–414, 2006.

Yu, X., Park, S. K., Lee, Y. H., and Choi, Y. S.: Quantitative precipitation forecast of a tropical cyclone through optimal parameter estimation in a convective parameterization, Sci. Online Lett. Atmos., 9, 36–39, 2013.

Zeweldi, D. A. and Gebremichael, M.: Evaluation of CMORPH precipitation products at fine space-time scales, J. Hydrometeorol., 10, 300–307., 2009.

Zhou, T.-J. and Yu, R.-C.: Atmospheric water vapor transport associated with typical anomalous summer rainfall patterns in China, J. Geophys. Res., 110, D08104, doi:10.1029/2004JD005413, 2005.

Table 1. Classification of precipitation types with the number of events (in bold).

		The portion of weather stations with precipitation (C1)	
		< 20 %	≥ 20 %
The station average precipitation rate (C2)	< 3 mm h^{-1}	Low Precipitation at a Few Points (LPFP) **5858**	Low Precipitation at Many Points (LPMP) **1157**
	≥ 3 mm h^{-1}	High Precipitation at a Few Points (HPFP) **980**	High Precipitation at Many Points (HPMP) **594**

Table 2. Monthly occurrences of precipitation systems according to the precipitation types from April to October in the period of 2013–2015.

	LPMP	HPMP	HPFP
APR	277	31	21
MAY	106	54	37
JUN	130	50	186
JUL	191	213	250
AUG	193	158	326
SEP	138	56	116
OCT	122	32	44

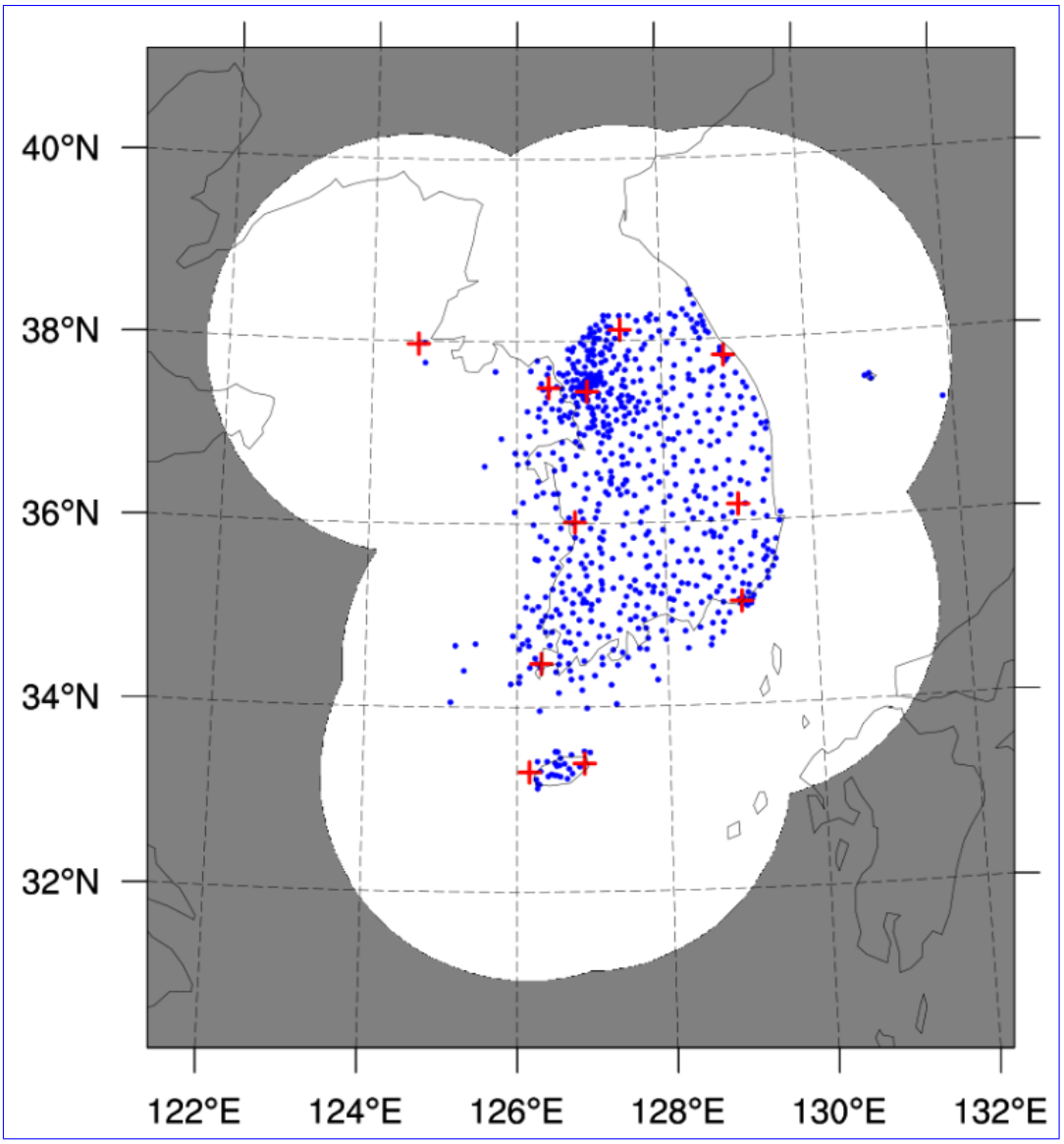

Figure 1. The weather station locations ~~of AWS stations~~ (blue dots) and radar locations (red "+" symbols) and coverages (white area) in Korea.

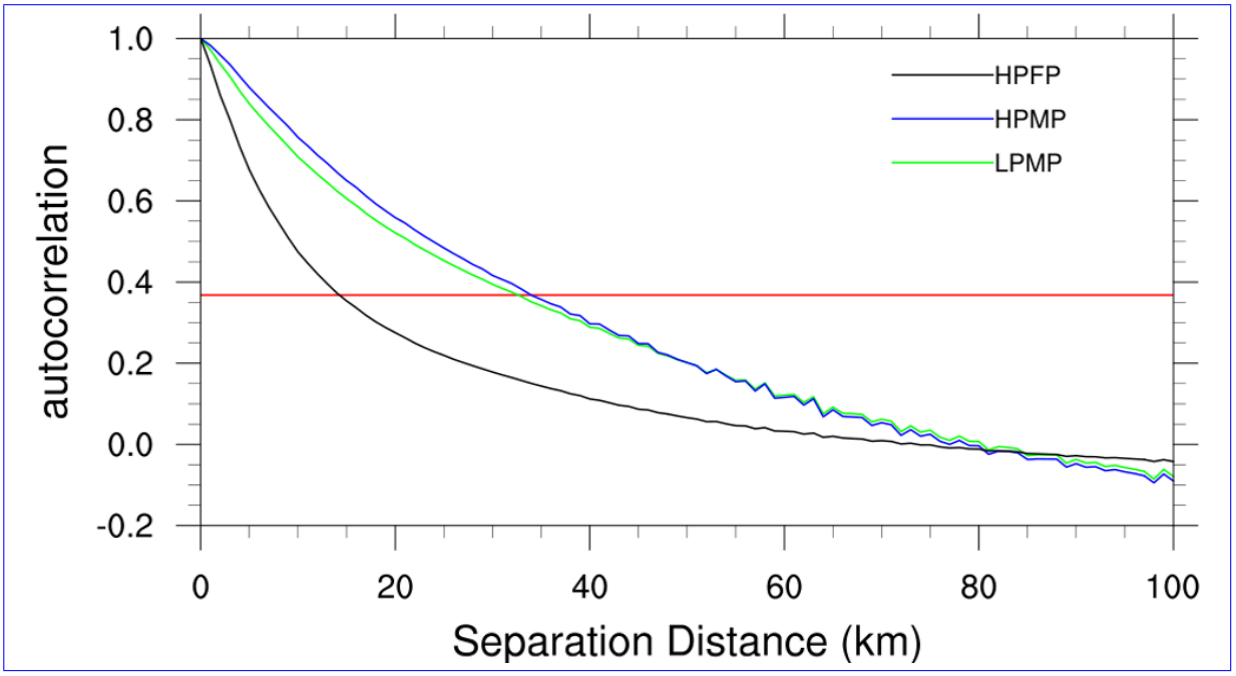

Figure 2. The averaged spatial autocorrelations of precipitation for each precipitation type. The red line indicates the *e*-folding value.

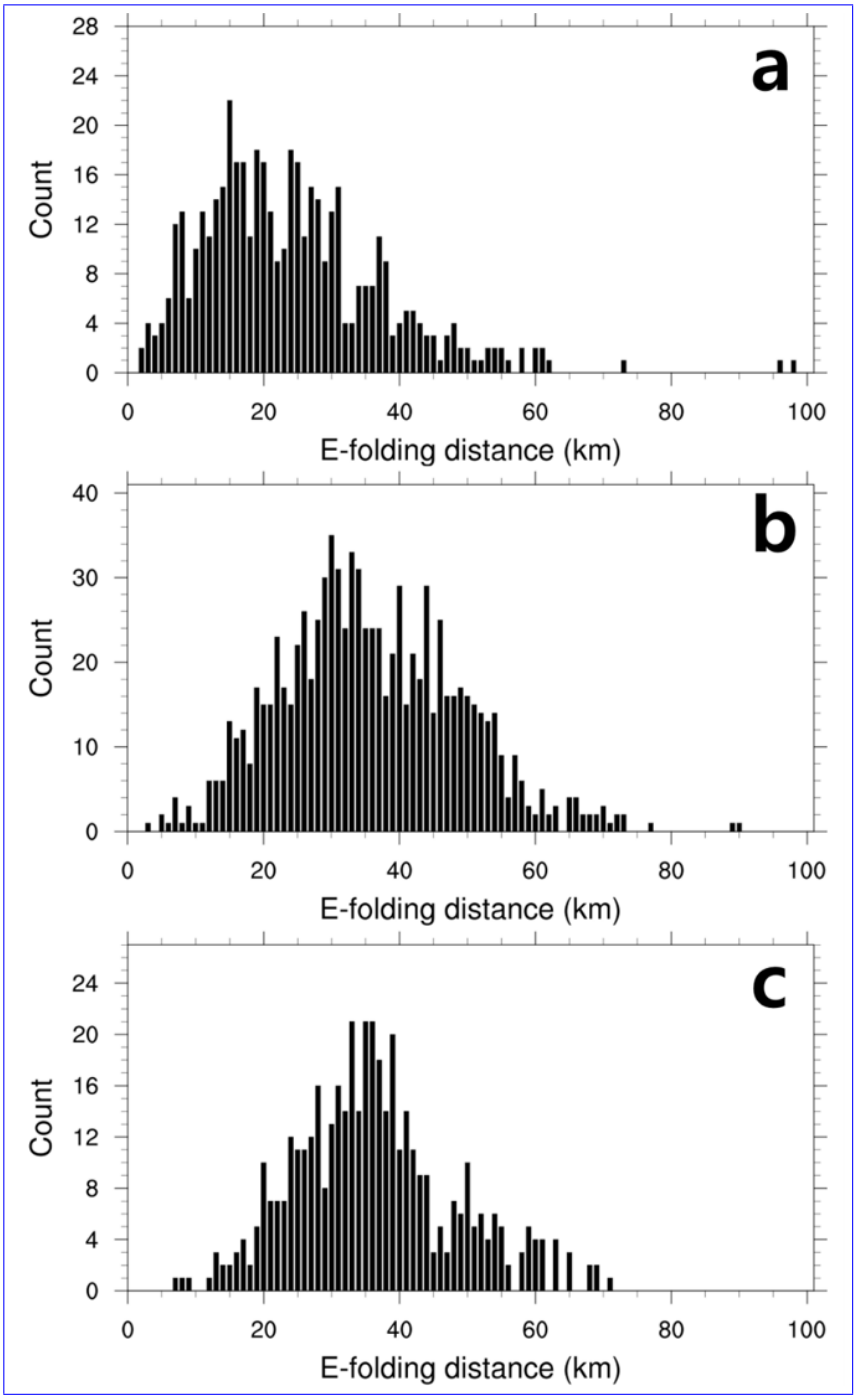

Figure 3. A histogram depicting the number of cases according to the *e*-~~folding~~ -folding distance for (a) HPFP, (b) LPMP, and (c) HPMP.

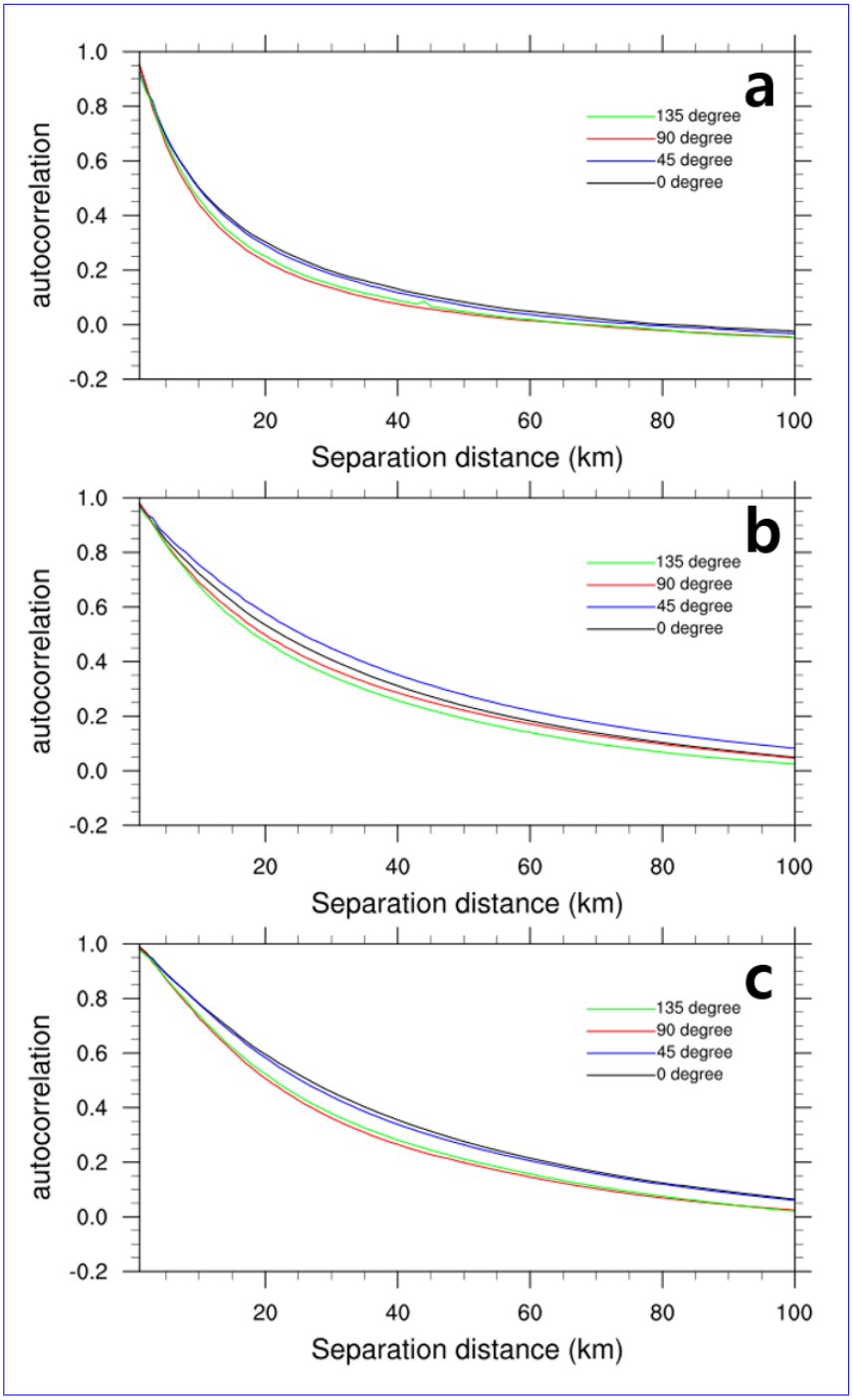

Figure 4. The averaged directional spatial autocorrelation of precipitation for (a) HPFP, (b) LPMP, and (c) HPMP.

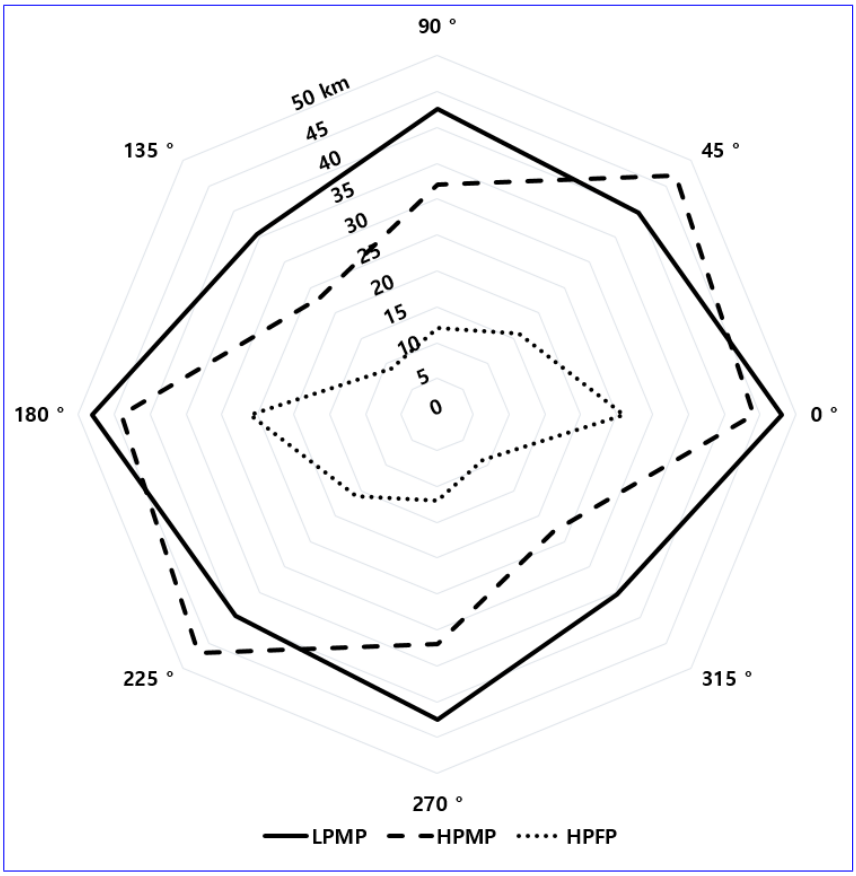

Figure 5. A radar ~~diagram~~ chart representing the directional *e*~~-folding~~ -folding distance (in km) for each precipitation type at the mode in the directional histogram (not shown) depicting the number of cases according to the *e*~~-folding~~ -folding distance in different directions.

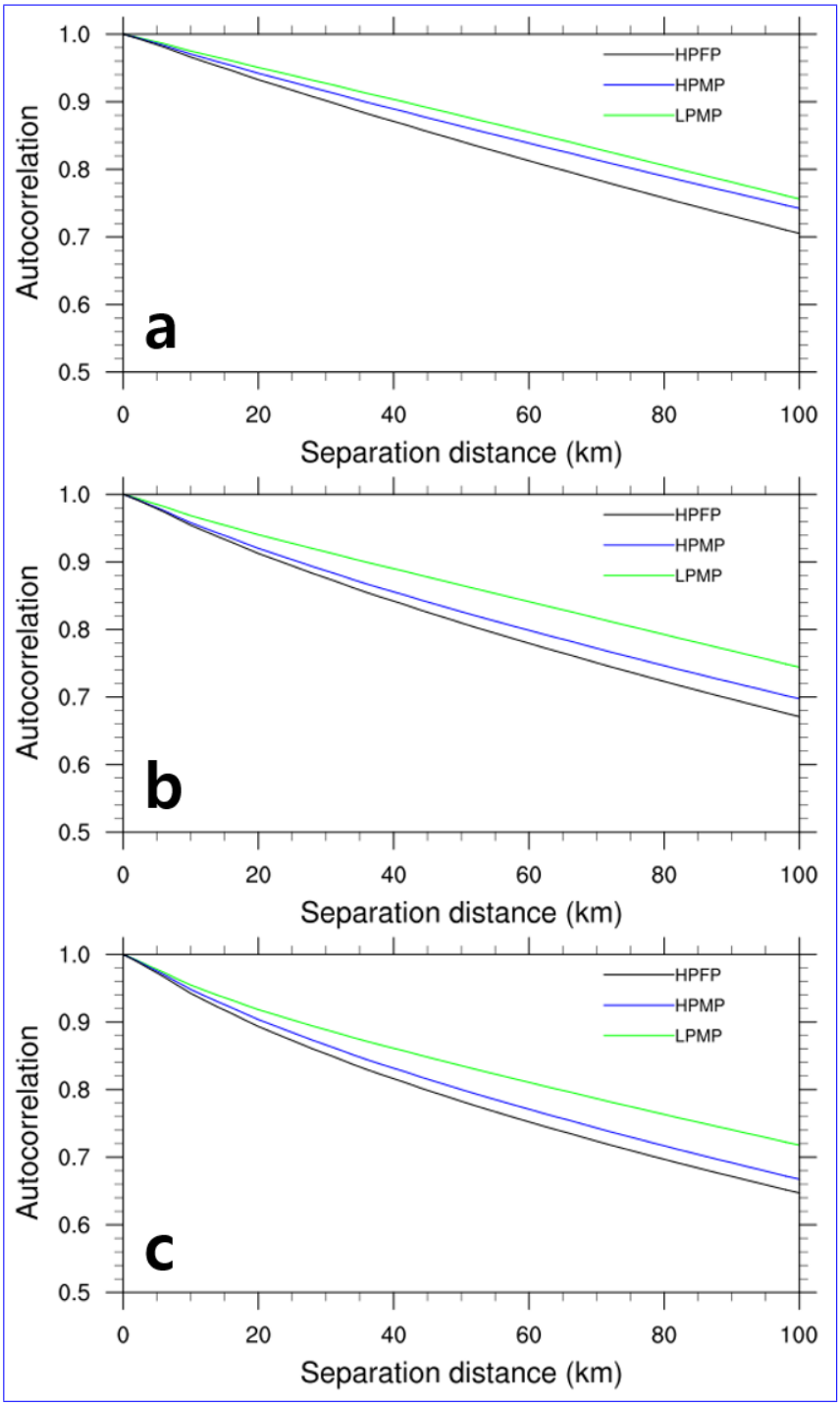

Figure 6. The averaged spatial autocorrelation of brightness temperature of the Himawari/AHI water vapor band (a) 8, (b) 9, and (c) 10 for each precipitation type.

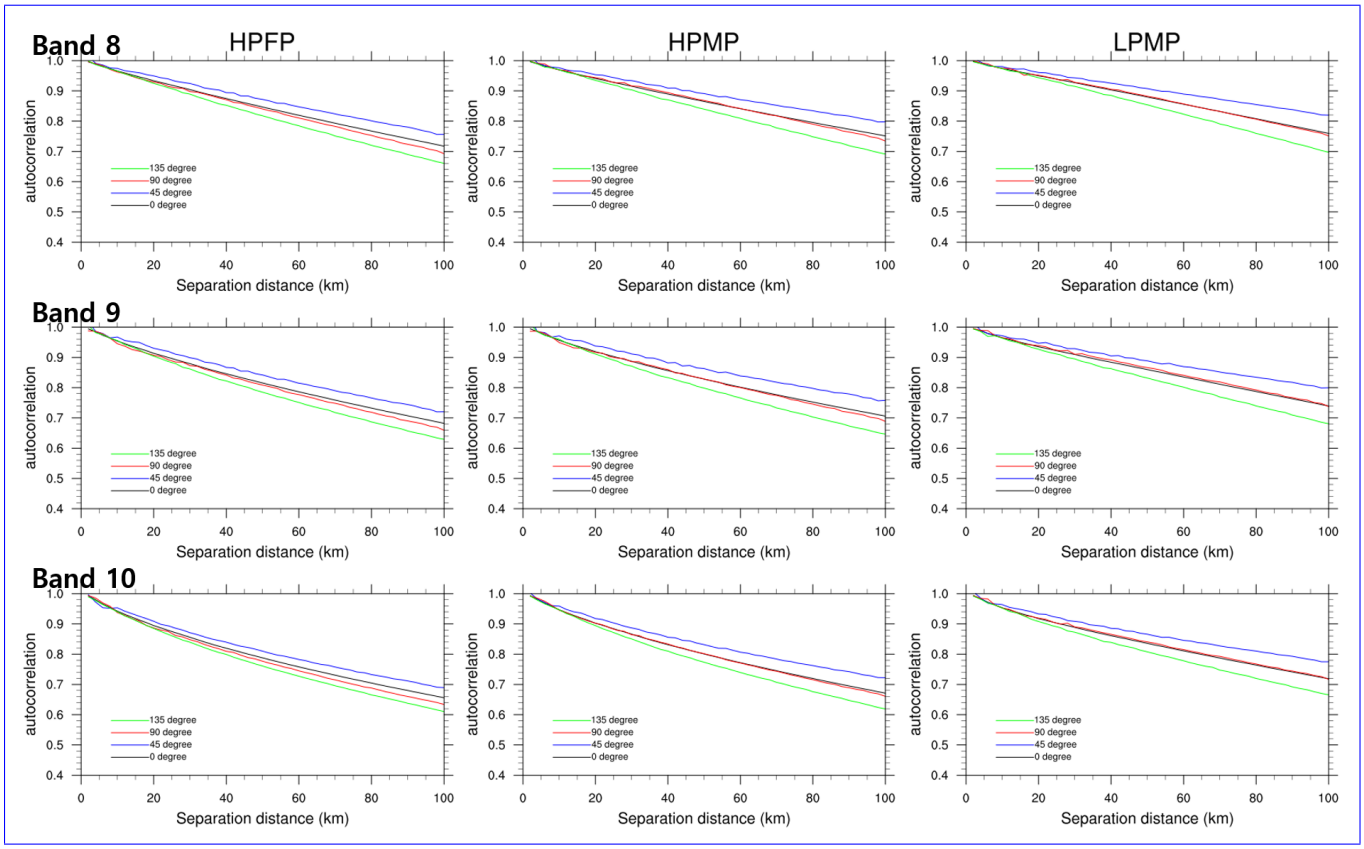

Figure 7. The averaged directional spatial autocorrelation of the brightness temperature of ~~three~~ the Himawari/AHI water vapor ~~bands for~~ band 8, 9 and 10 by each precipitation type (i.e., HPFP, HPMP, and LPMP) for directions of 0° (black), 45° (blue), 90° (red), and 135° (green). The direction (angle) is measured counterclockwise from the origin–east axis (i.e., 0°).

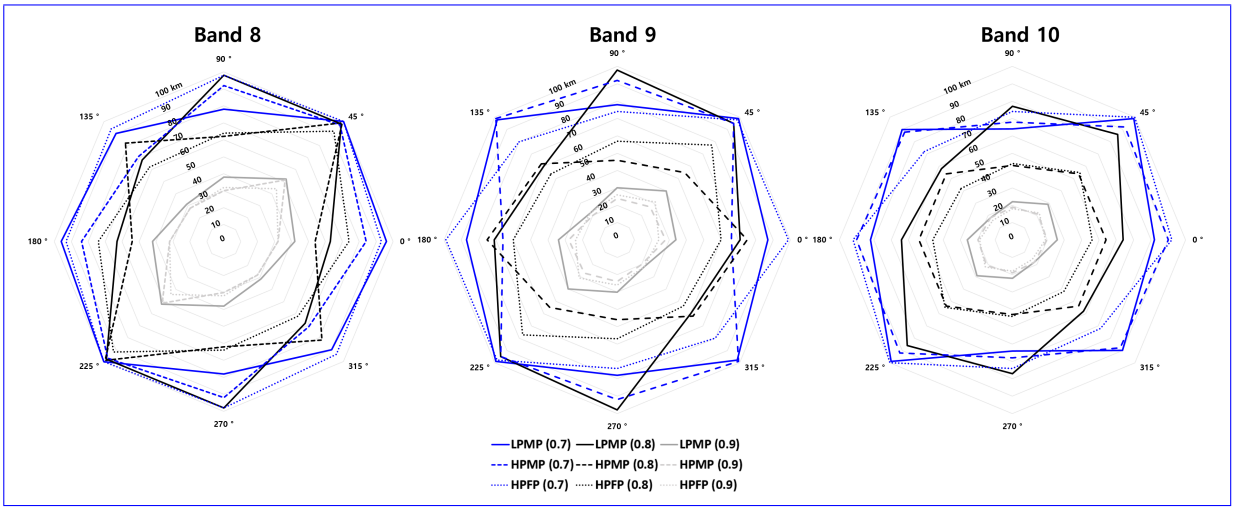

Figure 8. A radar ~~diagram depicting~~ chart representing the directional separation distance (in km) of brightness temperature of the Himawari/AHI water vapor ~~bands with~~ band 8, 9, and 10 at the mode in the histogram of case numbers for LPMP (solid), HPMP (dashed), and HPFP (dotted). The colors indicate autocorrelation ~~coefficient~~ coefficients of 0.7 (blue), 0.8 (black), and 0.9 (grey)~~. The precipitation types~~, ~~LPMP, HPMP and HPFP, are represented by solid, dashed, and dotted lines,~~ respectively.

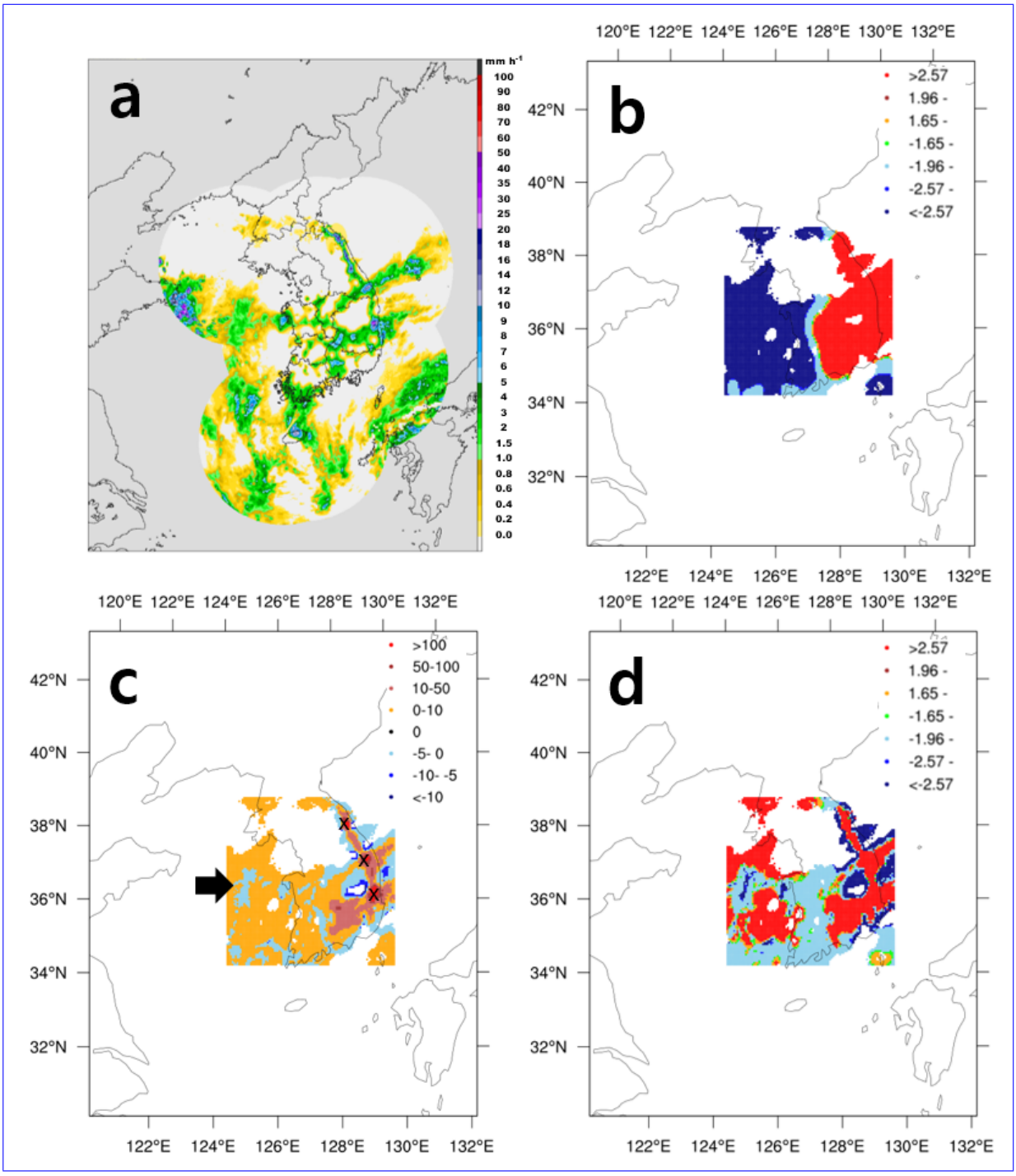

Figure 9. An LPMP case at 05 KST 25 August 2015: (a) Precipitation distribution (from https://afso.kma.go.kr/), (b) local ~~$Z(G_i)$~~ $Z(G_i)$, (c) local Moran's I (I_i), and (d) ~~Z-score~~ Z-score of I_i ~~at 05 KST 25 August 2015. Single cell storms~~. The computational domain covers the area of 34.34–38.97°N and 124.25–130.05°E. Precipitation systems with maximum intensity and strong cluster characteristics are marked by the ~~crosses~~X symbols, and the cold spots with dispersion pattern are denoted by the arrow. Non-precipitating areas have no color shading.

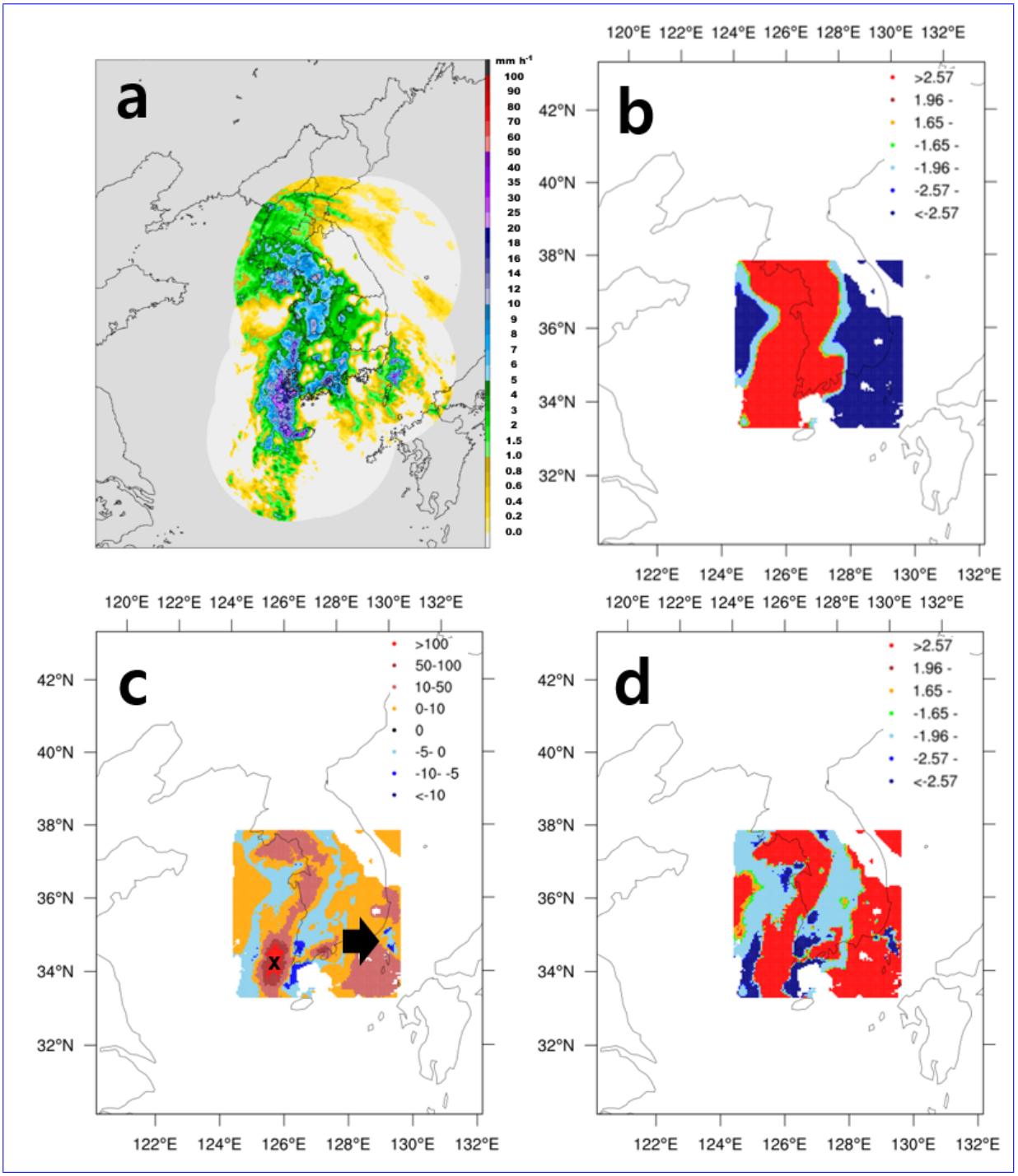

Figure 10. Same as in Fig. 9 but for an HPMP case at 17 KST 27 May ~~2013.~~2013 and the computational domain of 33.43–38.05°N and 124.25–130.04°E.

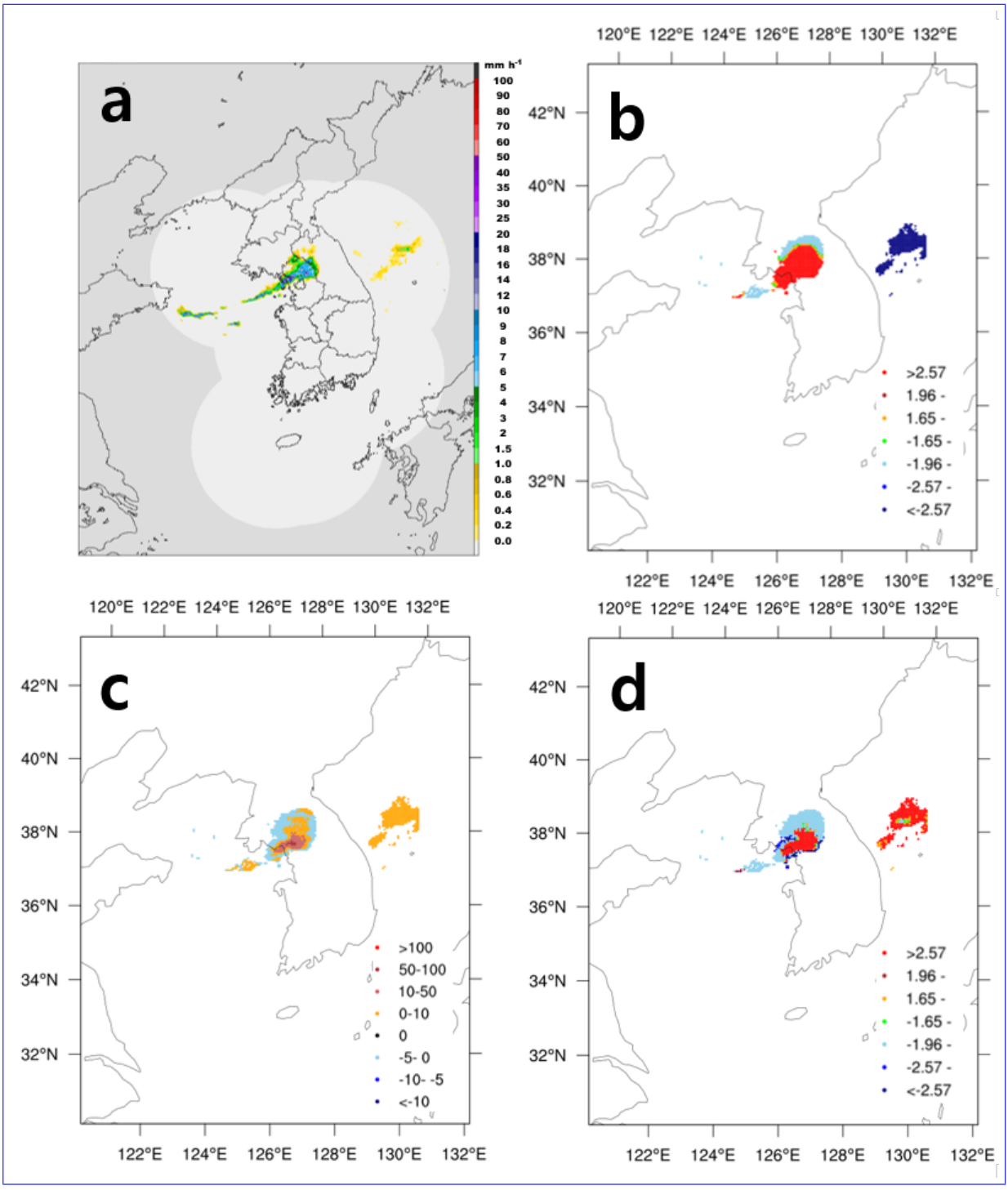

Figure 11. Same as in Fig. 9 but for an HPFP case at 05 KST 24 October ~~2015.~~2015 and the computational domain of 37.14–39.06°N and 123.32–131.21°E.

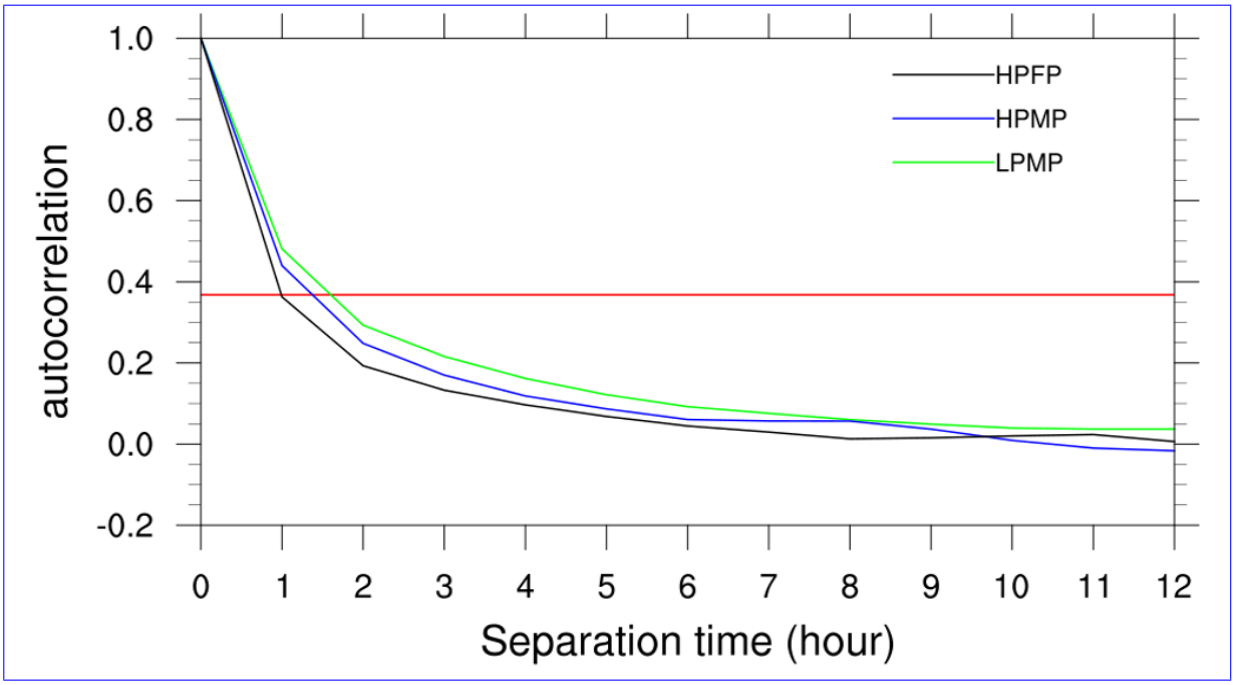

Figure 12. Same as in Fig. 2 but for the averaged temporal autocorrelation.

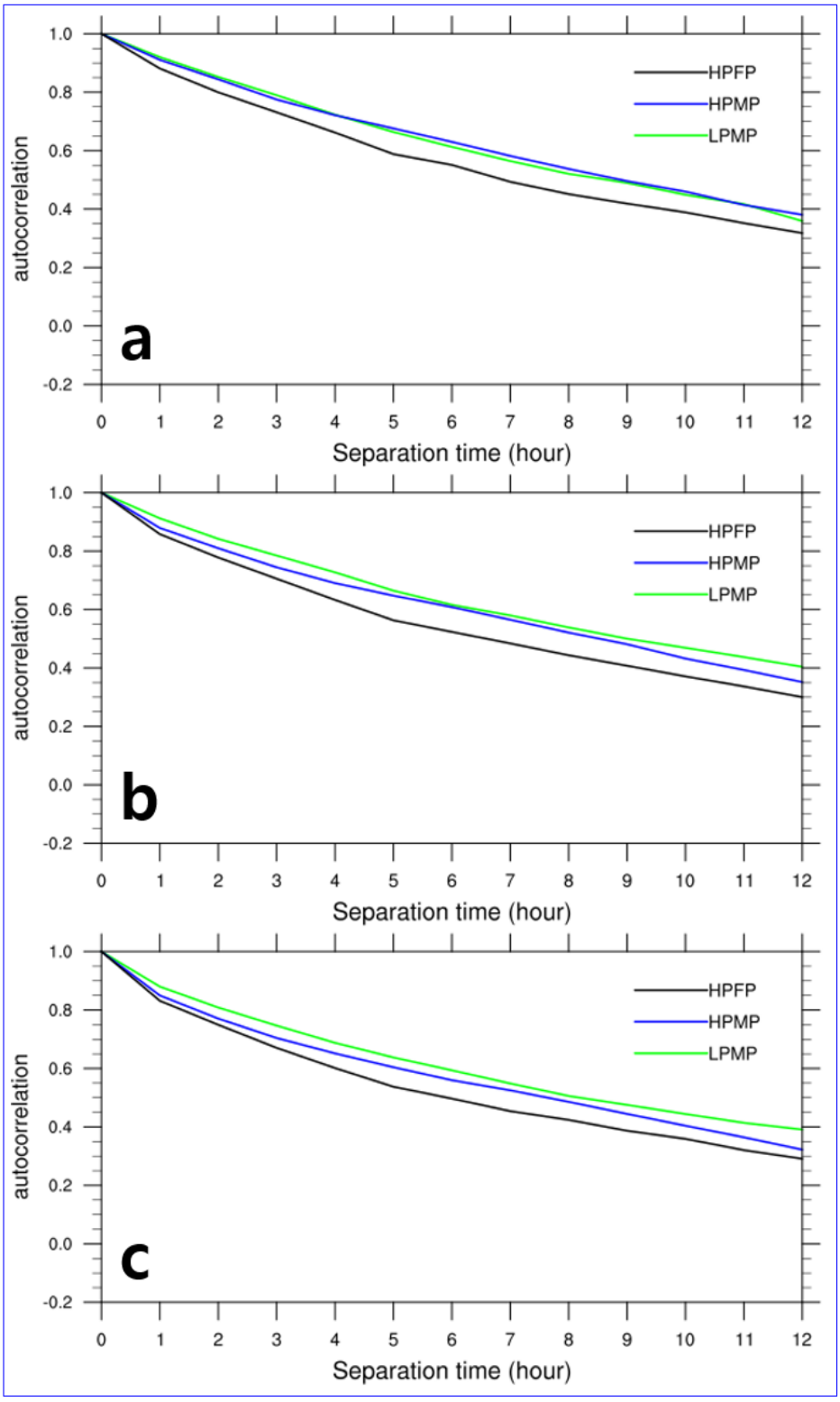

Figure 13. Same as in Fig. 6 but for the averaged temporal autocorrelation.